AML1 mutations induced MDS and MDS/AML in a mouse BMT model

Naoko Watanabe-Okochi,[1] Jiro Kitaura,[1] Ryoichi Ono,[1] Hironori Harada,[2] Yuka Harada,[3] Yukiko Komeno,[1] Hideaki Nakajima,[1] Tetsuya Nosaka,[1] Toshiya Inaba,[4] and Toshio Kitamura[1]

[1]Division of Cellular Therapy, Advanced Clinical Research Center, The Institute of Medical Science, The University of Tokyo, Tokyo; [2]Department of Hematology and Oncology, Research Institute for Radiation Biology and Medicine, Hiroshima University, Hiroshima; [3]International Radiation Information Center, Research Institute for Radiation Biology and Medicine, Hiroshima University, Hiroshima; and [4]Department of Molecular Oncology, Research Institute for Radiation Biology and Medicine, Hiroshima University, Hiroshima, Japan

Myelodysplastic syndrome (MDS) is a hematopoietic stem-cell disorder characterized by trilineage dysplasia and susceptibility to acute myelogenous leukemia (AML). Analysis of molecular basis of MDS has been hampered by the heterogeneity of the disease. Recently, mutations of the transcription factor AML1/RUNX1 have been identified in 15% to 40% of MDS–refractory anemia with excess of blasts (RAEB) and MDS/AML. We performed mouse bone marrow transplantation (BMT) using bone marrow cells transduced with the *AML1* mutants. Most mice developed MDS and MDS/AML-like symptoms within 4 to 13 months after BMT. Interestingly, among integration sites identified, Evi1 seemed to collaborate with an *AML1* mutant harboring a point mutation in the Runt homology domain (D171N) to induce MDS/AML with an identical phenotype characterized by marked hepatosplenomegaly, myeloid dysplasia, leukocytosis, and biphenotypic surface markers. Collaboration between AML1-D171N and *Evi1* was confirmed by a BMT model where coexpression of AML1-D171N and *Evi1* induced acute leukemia of the same phenotype with much shorter latencies. On the other hand, a C-terminal truncated *AML1* mutant (S291fsX300) induced pancytopenia with erythroid dysplasia in transplanted mice, followed by progression to MDS-RAEB or MDS/AML. Thus, we have developed a useful mouse model of MDS/AML that should help in the understanding of the molecular basis of MDS and the progression of MDS to overt leukemia. (Blood. 2008;111:4297-4308)

Introduction

Myelodysplastic syndromes (MDS) are a heterogeneous group of clonal stem-cell disorders characterized by ineffective hematopoiesis and susceptibility to leukemic transformation (MDS/acute myelogenous leukemia [AML]). Progression from MDS-refractory anemia with excess blasts (MDS-RAEB) to AML is frequently observed in the clinical course, which is thought to result from serial acquisition of cytogenetic abnormalities.[1-5] According to the 2-hit model of leukemogenesis, one class of mutations (class I), including FLT3-ITD, N-Ras, or K-Ras mutations, confers on cells a proliferative advantage; a second class of mutations (class II), including AML1/ETO, PML/RARα, or MLL-related fusion genes, interferes with hematopoietic differentiation.[6] Indeed, it has been reported that a combination of class I and II mutations such as FLT3-ITD plus AML1-ETO or MLL-SEPT6 induced AML in a mouse bone marrow transplantation (BMT) model, while either class I or II mutations alone led to, if anything, myeloproliferative disorders (MPDs), not leukemia.[6-13] On the other hand, the precise molecular mechanism underlying development of MDS and MDS/AML remains elusive partly because there are only a few mouse models for MDS and MDS/AML available. So far, 2 distinct models of MDS have been reported: *Evi1* induced MDS-like symptoms in a mouse BMT model in which the mice succumbed to fatal peripheral cytopenia,[14] while NUP98-HOXD13 transgenic mice developed MDS and died of either various types of acute leukemia or severe anemia and leukocytopenia.[15] In the present study, we generated a mouse BMT model of MDS-RAEB and MDS/AML induced by *AML1* mutants frequently found in patients with MDS and MDS/AML. Interestingly, the phenotypes of these mice very much resemble those of the human diseases.

The *AML1* gene is located on chromosome 21q22 and is the most frequent target for chromosomal translocation in leukemia. Analysis of AML1-deficient mice has shown that *AML1* is indispensable for the establishment of definitive hematopoiesis.[16-18] As accumulated studies have demonstrated, heterozygous germline mutations in the *AML1* gene caused familial platelet disorder with predisposition to AML (FPD/AML),[19,20] and sporadic point mutations were frequently found in the development of leukemia: 21% of AML M0, 15.0% to 15.9% of MDS-RAEB and MDS/AML, and 46% of radiation-associated MDS.[21-29] The vast majority of AML1 mutations were located in the Runt homology domain (RHD), which mediated its ability to bind to DNA and core-binding factor β (CBFβ). To confirm the involvement of *AML1* mutations in hematopoietic disorders, we selected 2 types of *AML1* mutants found in patients with MDS/AML: one with a point mutation in RHD (AML1-D171N), and the other with C-terminal truncation caused by a frame-shift (AML1-S291fsX300). After transplantation using bone marrow cells infected with retrovirus vectors harboring *AML1* mutants, most of the mice that received transplants died of MDS-RAEB and MDS/AML. Long-term analysis demonstrated that the phenotype of the mice that underwent

Submitted January 15, 2007; accepted December 24, 2007. Prepublished online as *Blood* First Edition paper, January 11, 2008; DOI 10.1182/blood-2007-01-068346.

An Inside *Blood* analysis of this article appears at the front of this issue.

The online version of this article contains a data supplement.

The publication costs of this article were defrayed in part by page charge payment. Therefore, and solely to indicate this fact, this article is hereby marked "advertisement" in accordance with 18 USC section 1734.

transplantation depended on the kind of *AML1* mutants used in this study and on the integration sites of retroviruses. Considering the recent reports of the effects of retrovirus integration sites on biological results,[30-38] identification of integration sites may lead to the discovery of the genes involved in the induction of MDS/AML in concert with *AML1* mutants. Intriguingly, the enhanced expression of Evi1 by retrovirus integration seemed to collaborate with AML1-D171N to induce MDS/AML with the same phenotype. Moreover, we confirmed that combination of AML1-D171N and *Evi1* induced AML of the same phenotype with shorter latencies in the mouse BMT model. This model will allow valuable insight into the molecular pathogenesis of MDS and MDS/AML.

Methods

Vector construction

We used 2 *AML1* mutants, D171N or S291fsX300, identified from case no. 5 or 27, respectively, among patients with MDS/AML.[25,26] These mutants are hereafter referred to as AML1-D171N and AML1-S291fs. AML1 wild-type (WT; AML1b), AML1-D171N, or AML1-S291fs, which was fused with a FLAG epitope tag at the N-terminus, was inserted upstream of the IRES-EGFP cassette of pMYs-IG to generate pMYs-AML1 WT, D171N, or S291fs-IG, respectively. pMYs-mouse Evi1-IG were kindly provided by Dr T. Nakamura (The Cancer Institute, Tokyo, Japan).[38]

Transfection and retrovirus production

Plat-E[39] packaging cells maintained in Dulbecco modified Eagle medium (DMEM) supplemented with 10% fetal calf serum (FCS) were transfected with retroviral constructs by using FuGENE 6 (Roche Diagnostics, Mannheim, Germany) according to the manufacturer's recommendations. The medium was changed 1 day after the transfection, and retroviruses were harvested 48 hours after the transfection as previously described.[39,40] Titers of the retroviruses were assessed based on the number of neomycin-resistant colonies of the infected NIH3T3 cells (average: 10^7 infection U/mL) as described.[39]

Mouse BMT

Bone marrow mononuclear cells were isolated from the femurs and tibias of C57BL/6 (Ly-5.1) donor mice (9-12 weeks of age) 4 days after intraperitoneal administration of 150 mg/kg 5-fluorouracil (5-FU) and cultured overnight in α minimal essential medium (αMEM) supplemented with 20% FCS and 50 ng/mL of mouse stem cell factor (SCF), mouse FLT3 ligand (FL), human IL-6, and human thrombopoietin (TPO; R&D Systems, Minneapolis, MN). The prestimulated cells were infected for 60 hours with the retroviruses harboring pMYs-AML1 WT, D171N, or S291fs-IG, or an empty vector as a control, using 6-well dishes coated with RetroNectin (Takara Bio, Shiga, Japan) according to the manufacturer's recommendations. Then, 0.2 to 3.5×10^6 of infected bone marrow cells (Ly-5.1) were injected through tail vein into C57BL/6 (Ly-5.2)–recipient mice (8-12 weeks of age) which had been administered a sublethal dose of 5.25 Gy or a lethal dose of 9.5 Gy total-body γ-irradiation (^{135}Cs). For the lethally irradiated mice, a radioprotective dose of 2×10^5 of bone marrow cells (Ly-5.2) was simultaneously injected. Probabilities of overall survival of the mice that received transplants were estimated using the Kaplan-Meier method. All animal studies were approved by the Animal Care Committee of the Institute of Medical Science, The University of Tokyo.

Analysis of the mice that underwent transplantation

Engraftment of bone marrow cells infected with retroviruses was confirmed by measuring the percentage of GFP$^+$ and Ly-5.1$^+$ cells in peripheral blood obtained every 1 to 2 months after the transplantation.

After the morbid mice were killed, their tissue samples, including peripheral blood (PB), bone marrow (BM), spleen, liver, and kidney, were analyzed. Circulating blood cells were counted by an analyzer. Morphology of the peripheral blood was evaluated by staining of air-dried smears with Hemacolor (Merck, Darmstadt, Germany). Tissues were fixed in 10% buffered formalin, embedded in paraffin, sectioned, and stained with hematoxylin and eosin (H&E). Cytospin preparations of bone marrow and spleen cells were also stained with Hemacolor. Percentage of blasts, myelocytes, neutrophils, monocytes, lymphocytes, and erythroblasts was estimated by examination of at least 200 cells. To assess whether the leukemic cells were transplantable, 2×10^5 to 10^6 total BM cells including blasts were injected into the tail veins of sublethally irradiated mice. A total of 2 or 3 recipient mice were used for each serial transplantation.

Flow cytometric analysis

Red blood cells were lysed by using Ammonium Chloride Lysing Reagent (BD Biosciences, San Jose, CA) in PB or single-cell suspensions of bone marrow and spleen. Washed cells were incubated for 15 minutes at 4°C with 2.4G2 antibody for blocking and then stained for 20 minutes at 4°C with the following monoclonal phycoerythrin (PE)–conjugated antibodies: Ly-5.1, Gr-1, CD11b, B220, CD3, CD41, c-Kit, Sca-1, CD34, and Ter119. Flow cytometric analysis of the stained cells was performed with FACSCalibur flow (BD Biosciences) equipped with CellQuest software (BD Biosciences) and Flowjo software (Tree Star, San Carlos, CA).

Diagnosis

Diagnosis was made according to the Bethesda proposals for classification of nonlymphoid hematopoietic neoplasms in mice.[41]

Real-time RT-PCR

Total RNA was extracted from BM cells using Trizol (Invitrogen, Carlsbad, CA). cDNA was prepared with the Superscript II RT kit (Invitrogen). Real-time reverse transcription–polymerase chain reaction (RT-PCR) was performed using a LightCycler Workflow System (Roche Diagnostics). cDNA was amplified using a SYBR Premix EX Taq (TAKARA). Reaction was subject to one cycle of 95°C for 30 seconds, 45 cycles of PCR at 95°C for 5 seconds, 55°C for 10 seconds, and 72°C for 10 seconds. All samples were independently analyzed at least 3 times. The following primer pairs were used: 5′-CCAGATGTCACATGACAGTGGAAAGCACTA-3′ (forward) and 5′-CCGGGTTGGCATGACTCATATTAACCATGG-3′ (reverse) for Evi1; 5′-TACCTCAACCCCTGACAGCTATGG-3′ (forward) and 5′-TCGGTTGGAGATATCAGAGTGCAG-3′ (reverse) for MN1;[42] and 5′-GTTATCCCATCTGCATCAGCATCTGG-3′ (forward) and 5′-GGTCCTCTTCACTCTTCATGAACAGC-3′ (reverse) for MDS1/Evi1.[43] Relative gene expression levels were calculated using standard curves generated by serial dilutions of cDNA. Product quality was checked by melting curve analysis via LightCycler software (Roche Diagnostics). Expression levels were normalized by a control, the expression level of GAPDH mRNA.

Western blot analysis

To detect the expression of *AML1* WT, mutants, or *Evi1*, equal numbers of spleen cells were lysed, and Western blotting was performed as described with minor modifications.[13] Polyclonal rabbit anti-Evi1 antibody (a kind gift from Dr M. Kurokawa, Tokyo University, Tokyo, Japan), or a monoclonal mouse anti-Flag antibody (Sigma-Aldrich, St Louis, MO) was used for *Evi1* or *AML1*, respectively.

Southern blot analysis

Genomic DNA was extracted from BM or spleen cells. After enzymatic digestion of 10 μg DNA with *Eco*RI followed by electrophoretic separation, proviruses were probed with a GFP probe.

Bubble PCR

A total of 10 μg of genomic DNA extracted from BM or spleen cells was digested with *Eco*RI, and the fragments were ligated overnight at 16°C to a double-stranded bubble linker (5′-AATTGAAGGAGAGGACGCTGTCTG-

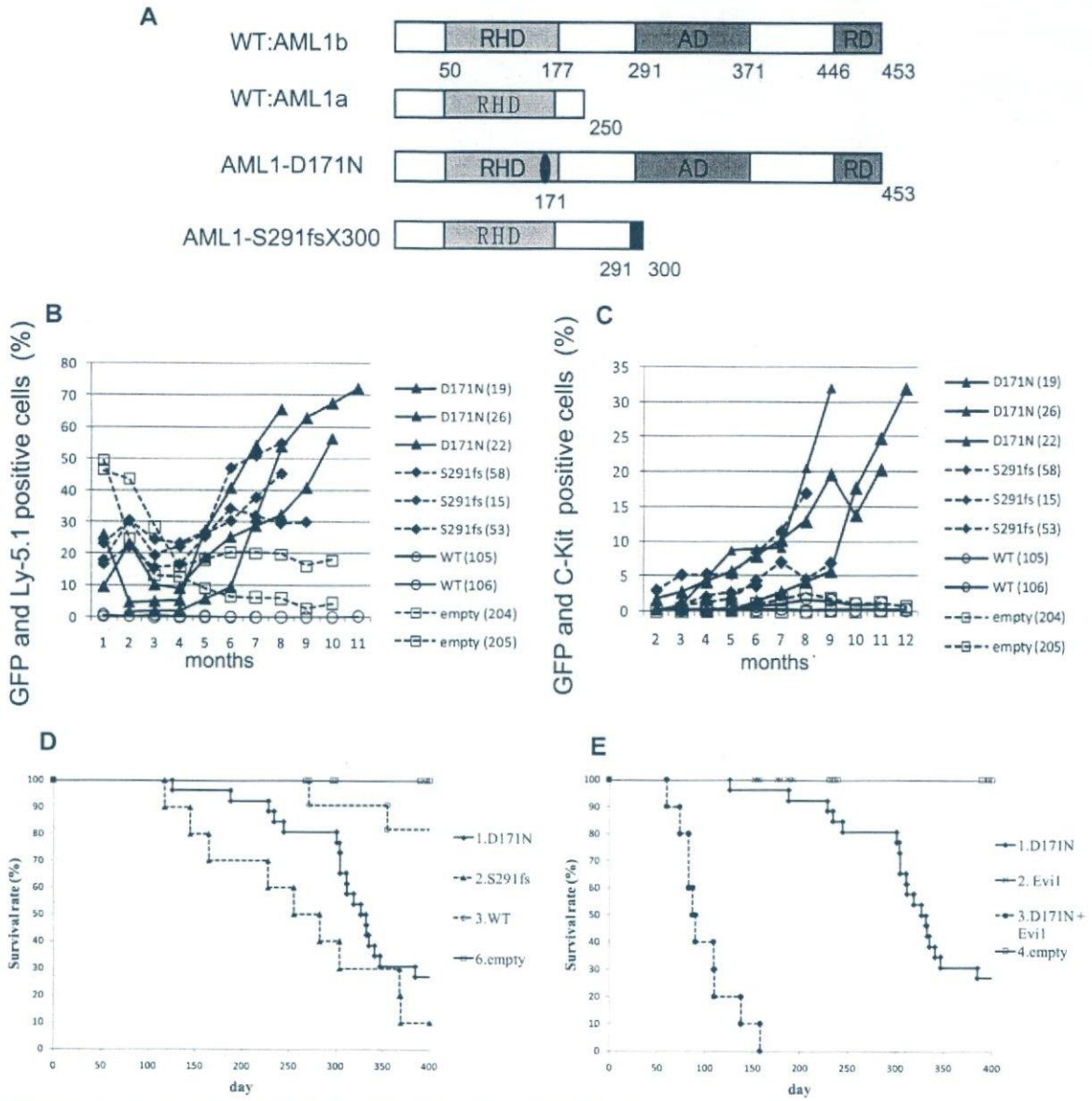

Figure 1. MDS and MDS/AML induced by *AML1* mutants derived from patients with MDS. (A) Schematics of *AML1* WT (AML1a and AML1b) and *AML1* mutants (D171N and S291fs). AD indicates transactivating domain; RD, repression domain. (B) Percentages of GFP/Ly-5.1 double-positive cells or (C) c-Kit$^+$ cells in PB. PB was obtained from the tail vein every month after the transplantation. Numbers in parenthesis indicate mouse IDs. (D) Kaplan-Meier analysis for the survival of mice that received transplants of *AML1* mutant-transduced BM cells. Average survival days of AML1-D171N (340.6 days) were compared with AML1-S291fs (263.6 days) using the log-rank test; $P = .218$. AML1 WT (n = 11), D171N (n = 26), S291fs (n = 10), mock (n = 16). (E) Evi1 synergized with AML1-D171N in inducing MDS/AML. D171N (n = 26; same as those in panel D), *Evi1* (n = 8), D171N + *Evi1* (n = 10), and mock (n = 16) transduced bone marrow cells were transplanted into mice.

TCGAAGGTAAGGAACGGACGAGAGAAGGGAGAG-3′ and 5′-GACTC-TCCCTTCTCGAATCGTAACCGTTCGTACGAGAATCGCTGTCCTCTCC-TTC-3′).[44] Next, PCR was performed on the ligation product using a linker-specific Vectorette primer (5′-CGAATCGTAACCGTTCGTACGAGAATCGCT-3′)[44,45] and a long-terminal repeat (LTR)–specific primer (5′-CGAGCTCAATAAAA-GAGCCCACAACCCC-3′) under the following conditions: one cycle of 95°C for 5 minutes, 10 cycles of 95°C for 30 seconds, and 67°C for 30 seconds and 72°C for 3 minutes, 10 cycles of 95°C for 30 seconds, and 67°C (this annealing temperature was reduced by 1°C each cycle) for 30 seconds and 72°C for 3 minutes, 15 cycles of 95°C for 30 seconds and 57°C for 30 seconds and 72°C for 3 minutes, and one cycle of 72°C for 90 seconds. Next, nested PCR was performed on 2 μL of PCR products using a linker-specific Vectorette primer and an LTR-specific primer (5′-ATAAAAGAGCCCACAACCCCTCACTCGG-3′) under the following conditions: 1 cycle of 95°C for 5 minutes, 35 cycles of 95°C for 30 seconds and 60°C for 30 seconds and 72°C for 3 minutes, and 1 cycle of 72°C for 90 seconds. The PCR product was electrophoresed using 1.0% agarose gel. Individual bands were excised and purified using PCR clear (Promega, Madison, WI) and were sequenced to identify the integration site of retrovirus. We confirmed inverse repeat sequence "GGGGGTCTTTCA" as a marker of junction between genomic DNA and retrovirus sequence.

Results

The ratio of *AML1* mutant-transduced cells gradually increased over several months after transplantation

To examine the effect of *AML1* mutants on the hematopoietic abnormality, we chose 2 distinct mutants, AML1-D171N and AML1-S291fsX300, which are found in patients with MDS/

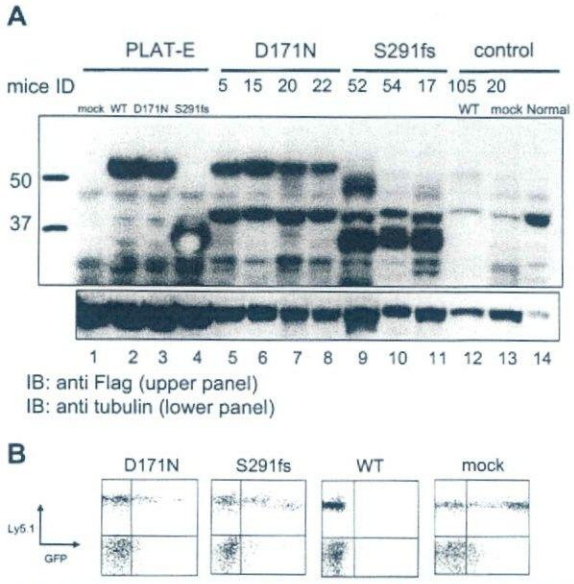

Figure 2. Expression of the transduced AML1-D171N, AML1-S291fs, and AML1 WT in spleen of the transplanted mice. (A) Lysates of spleen cells were immunoblotted with anti-Flag Ab. As a positive control, Plat-E packaging cells were transduced with mock (lane 1), AML1 WT (lane 2), AML1-D171N (lane 3), or AML1-S291fs (lane 4). Spleen cells were derived from mice/D171N (lanes 5-8), mice/S291fs (lanes 9-11), mice/WT (lane 12), mice/mock (lane 13), or control normal mouse (lane 14). White arrows indicate transduced AML1 WT, AML1-D171N, and AML1-S291fs. (B) AML1 WT-transduced cells were undetectable in PB at 1 month after the transplantation. Flow cytometric analysis of PB obtained from mice that received transplants of AML1-D171N, AML1-S291fs, AML1 WT, and mock at 1 month after transplantation.

AML.[25,26] The former has a point mutation in RHD, and the latter possesses a frameshift mutation in the C-terminal region, resulting in truncation of the authentic protein (Figure 1A). Ly-5.1 murine BM cells infected with retroviruses harboring AML1 WT, AML1-D171N, AML1-S291fsX300, or empty vector were transplanted into irradiated syngeneic Ly-5.2 mice. In most of mice that received transplants of AML1-D171N– or S291fsX300-transduced cells (hereafter referred to as mice/D171N or mice/S291fs, respectively), the ratio of GFP$^+$ and Ly-5.1$^+$ cells gradually increased over several months after the transplantation (Figure 1B), but not in mice that received transplants of AML1 WT-transduced cells or control retrovirus-infected cells (hereafter referred to as mice/WT or mice/mock, respectively). Gradual increase of c-kit$^+$ cells in the PB was also observed in the mice that received transplants of *AML1* mutant-transduced cells during the observation period (Figure 1C). Cells positive for c-kit and GFP—that is, c-kit$^+$ cells transduced with *AML1* mutants—were morphologically blasts with high nuclear-cytoplasmic ratios (data not shown). In fact, the percentage of blasts gradually increased in the PB of the mice that received transplants of *AML1* mutant-transduced cells, especially the mice/D171N. Finally, most of mice/D171N or mice/S291fs became sick and died with latencies of 4 to 13 months after the transplantation, while mice/mock were healthy over the observation period (Figure 1D). Overall survival of mice/D171N was not significantly different from that of mice/S291fs ($P = .218$). Expression of the transduced AML1-D171N or AML1-S291fs in spleen cells was confirmed by Western blot analysis (Figure 2A). Two of the mice/WT died during the observation period. BM of the 2 mice was occupied with GFP/Ly5.1 double-negative cells. One of the mice/WT developed leukemia derived from recipient cells at 272 days after transplantation. The remaining one mouse/WT died of anemia with unknown reason at 355 days after transplantation.

Interestingly, in the peripheral blood of mice/WT, GFP$^+$ cell counts were extremely low 1 month after transplantation and thereafter became undetectable, despite the fact that 14% to 27% of the BM cells were positive for GFP before transplantation (Figures 1B,2B; Table S1, available on the *Blood* website; see the Supplemental Materials link at the top of the online article). Consistently, the expression of transduced AML1 WT was not detected in spleen cells of mice/WT (Figure 2A; mouse ID: 105). These data suggested that forced expression of AML1 WT in the stem cells had a negative effect on the survival and expansion of these cells in the BM. Recently, Tsuzuki et al reported that expression of the full-length isoform AML1b abrogated engraftment potential of murine long-term reconstituting stem cells in a mouse BMT model.[46] Their result coincides with our result.

AML1-D171N and AML1-S291fs induced different diseases in mice that underwent transplantation

PB cell counts were different between mice/D171N and mice/S291fs; most mice/D171N (Figure 3A; lanes 1,2) showed leukocytosis, while mice/S291fs (Figure 3A; lane 3) showed leukocytopenia. This difference was significant ($P = .007$). Macroscopic observation of morbid mice revealed that severe hepatosplenomegaly was exclusively found in mice/D171N, but not in mice/S291fs (Figure 3E,F; Table S2).

The smear specimens of peripheral blood were obtained every 1 to 2 months. The specimens showed that most of mice/D171N and mice/S291fs suffered from multilineage dysplasia characteristic of MDS. Erythroid dysplasia such as Howell-Jolly bodies, red cell polychromasia, and poikilocytosis (Figure 4A) were frequently detected in both mice. In BM specimens of morbid mice, orthochromatic giant erythroblasts and karyorrhexis were detected (Figure 4B). Erythroid dysplasia was more evident in mice/S291fs than in mice/D171N. As recently described in a mouse MDS model,[15] increase of red blood cell mean corpuscular volume (MCV) was also observed in most mice/D171N and mice/S291fs (Figure 3D; Table S2). Myeloid dysplasia such as the pseudo–Pelger-Huet anomaly (Figure 4C) was frequently detected in mice/D171N. Hypersegmented neutrophils (Figure 4D) and giant platelets (Figure 4F) were observed in 2 mice/D171N (mouse IDs 9 and 17). Collectively, *AML1* mutants used in this study induced multilineage dysplasia, in particular in erythroid and myeloid lineages. Continuous pancytopenia was observed in 7 of 8 morbid mice/S291fs and 2 of 16 morbid mice/D171N, although BM of the morbid mice was not hypocellular but hypercellular or normocellular. Based on these findings, a final diagnosis was made by the ratio of blasts in the bone marrow according to the Bethesda proposals for classification of nonlymphoid hematopoietic neoplasms in mice.[41] As a result, MDS/AML was recognized in 13 of 16 morbid mice/D171N and in 5 of 8 morbid mice/S291fs, while MDS-RAEB was recognized in 2 of 16 morbid mice/D171N and 2 of 8 morbid mice/S291fs (Table S2). One mouse/D171N was diagnosed with AML at 4 months after transplantation because we did not examine to see if the MDS phase had preceded AML (mouse ID 5). The leukemic cells derived from either mice/D171N or mice/S291fs were serially transplantable. We confirmed the serial transplantability in 11 mice/D171N (mouse IDs 4, 6, 9, 12-15, 17, 20, 22, and 26) and 6 mice/S291fs (mouse IDs 52, 54-56, 58, and 60). Penetrance of serial transplantation was 100%, except for mouse IDs 9 and 17; that is, 33% and 50%, respectively. Mice that underwent serial transplantation showed more aggressive status than primary mice

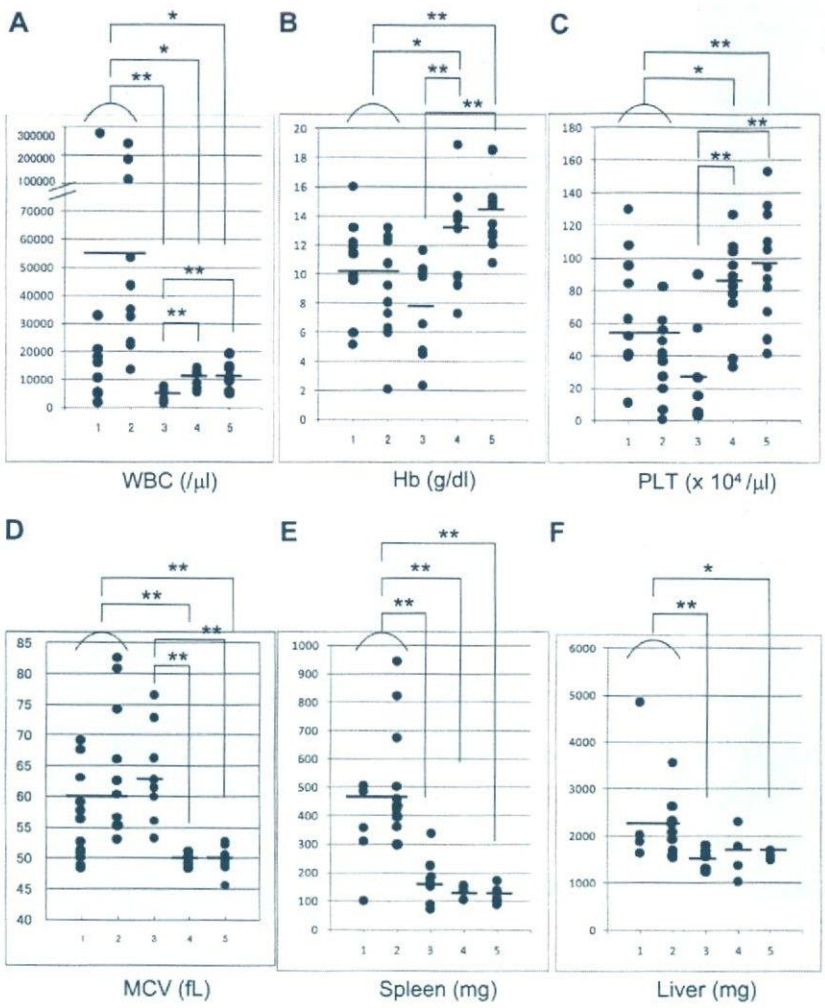

Figure 3. Peripheral white blood cell counts of mice/D171N showed leukocytosis, while mice/S291fs showed leukocytopenia. (A) Counts of white blood cells (WBCs) in PB. (B) Concentration of hemoglobin (Hg). (C) Counts of platelets (PLT). (D) Red cell MCV. (E,F) Weight of spleen and liver of morbid mice (mice/D171N or S291fs) or 1-year-old healthy mice (mice/WT or mock). Statistical differences were determined by 2-sample *t* test with Welch correction (*$P < .05$; **$P < .01$). Lane 1: mice/D171N without high expression of *Evi1* in BM or not examined due to the lack of bone marrow samples (WBC, PLT, Hg, and MCV: n = 11; spleen: n = 5; and liver: n = 4). Lane 2: mice/D171N with high expression of *Evi1* (n = 11). Lane 3: mice/S291fs (WBC, PLT, Hg, and MCV: n = 9; spleen and liver: n = 8). Lane 4: mice/WT (WBC, PLT, Hg, and MCV: n = 10; spleen and liver: n = 4). Lane 5: mice/mock (WBC, PLT, Hg, and MCV: n = 12; spleen: n = 6; and liver: n = 5).

and died with shorter latencies. Hematologic parameters of mice that underwent serial transplantation are shown in Table S3.

In summary, the pattern and degree of multilineage dysplasia differed among the mice that underwent transplantation. Although both mice/D171N and mice/S291fs died of MDS and MDS/AML within 4 to 13 months after transplantation, a marked difference existed in terms of clinical symptoms, including hematopoietic or macroscopic findings.

A distinct type of disease was identified in mice/D171N

Among the mice that underwent transplantation transduced with AML1-D171N, a distinct group was identified. GFP$^+$ BM cells in 11 of 16 morbid mice/D171N (mouse IDs 4, 6, 7, 12-15, 19, 20, 22, and 26) displayed a similar phenotype, with high percentages of CD11b$^+$ and B220$^+$ cells (Figure 5; data not shown). All these mice/D171N showed dysplasia in myeloid and erythroid lineages for several months and died of MDS/AML with increased number of blasts, anemia, and, in some cases, thrombocytopenia (Table S2). These mice/D171N also showed severe hepatosplenomegaly (Figures 3E,F, 6A; Table S2), and histologic examination showed expansion of blasts and immature myeloid cells in the PB, BM, and spleen, and the invasion of these cells into hepatic portal areas in the liver and spaces among renal tubules in the kidney (Figure 6B,D,F). Giemsa staining of BM showed a high percentage of blasts (Figure 6H), in accordance with a high percentage of both GFP/c-kit double-positive cells by flow cytometolic analysis.

In contrast, the remaining 4 morbid mice/D171N diagnosed as MDS (mouse IDs 9 and 11) or MDS/AML (mouse IDs 10 and 17) showed heterologous phenotypes of GFP$^+$ BM cells (data not shown). Although mouse IDs 9 and 17 displayed hepatosplenomegaly like other mice/D171N, they exhibited leukocytopenia with fewer blasts.

AML1-D171N collaborated with *Evi1* in inducing MDS/AML

We then asked why even the same point mutant of *AML1* caused different phenotypes of MDS-RAEB and MDS/AML. We assumed the possibility that the integration of retroviruses influenced the outcomes in the BMT model. To explore this, we first performed Southern blot analysis of BM of the morbid mice. A single or several proviral integrations were confirmed (Figure 7A). Next, we used the bubble PCR method to identify the integrated sites.[7,44,45] A single or 2 integration sites were identified in each sample (Table 1). Interestingly, integrations near *Evi1* site were found in 7 of 15 genomic DNA samples of BM cells derived from mice/D171N, but not from mice/S291fs. Moreover, retrospective examination revealed that these 7 mice presented nearly identical phenotypes, characterized by marked hepatosplenomegaly (Figure 6A), leukocytosis (Figure 3A), and biphenotypic surface markers (CD11b$^+$

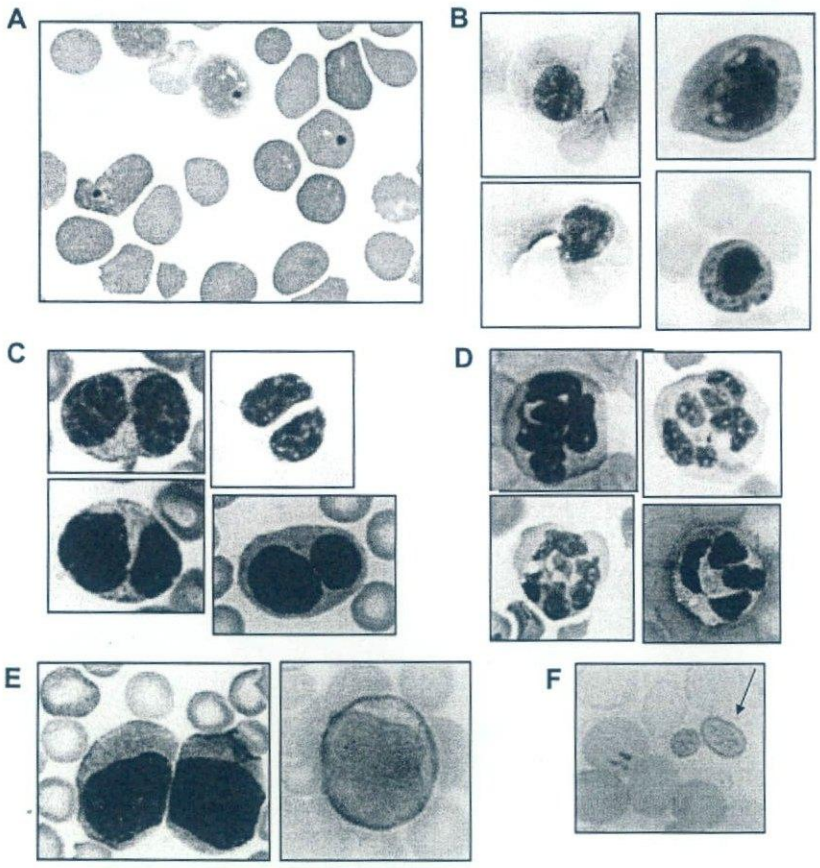

Figure 4. Multilineage dysplasia of hematopoietic cells in mice that received transplants of *AML1* mutants. Giemsa-stained PB smears obtained from mice/D171N or S291fs are shown. (A) Howell-Jolly body, polychromasia, and anisopoikilocytosis. (B) Orthochromatic giant erythroblast, karyorrhexis, and nuclear fragments. (C) Pseudo-Pelger-Huet anomaly. (D) Hypersegmented neutrophil. (E) Blasts in peripheral blood. (F) Giant platelet. Images were obtained with a BH51 microscope and DP12 camera (Olympus, Tokyo, Japan); objective lens, UPlanFl (Olympus); magnification, ×1000.

and B220$^+$) of the leukemic cells (Figure 5), thus constituting a definite subgroup among mice/D171N. Southern blot analysis showed that all of the leukemic mice with high expression of Evi1 are monoclonal (except for mouse IDs 15 and 19), but the other leukemic mice without high expression of Evi1 are oligoclonal or have several integrations (Figure 7A). Noteworthy was the finding that the *Evi1* site was not identified from the genomic DNA samples of mice/S291fs, even though the *Evi1* site is a known common integration site of retroviruses.[31-38] These led us to postulate that Evi1 collaborated with AML1-D171N in inducing the distinct type of MDS/AML. To test this, we examined whether the expression of *Evi1* was enhanced in the BM cells in which the integration into an *Evi1* site was identified. Real-time PCR analysis demonstrated that the expression levels of *Evi1* were high in all the related samples (Figure 7C). Protein expression levels corresponded to mRNA expression levels of Evi1 (Figure 7D; data not shown). Interestingly, 4 samples derived from mice/D171N harboring no integration near *Evi1* also displayed significantly high expression levels of *Evi1* (mouse IDs 13, 19, 20, and 22), and the phenotypes of these mice were identical to those induced by AML1-D171N–transduced cells in which retroviruses were integrated into the *Evi1* site. In these cases, the expression of *Evi1* might have been enhanced secondarily by an unknown mechanism, or we simply failed to detect the integration site. The latter possibility was supported by the fact that multiple integrations were detected in these cases (Figure 7A; mouse IDs 13, 19, and 20). In any case, all the mice/D171N with enhanced expression of Evi1 in their BM cells displayed high percentages of blasts (Figure S1). We also examined whether the expression of MDS1/Evi1 was enhanced by the integration into an *Evi1* site. The *MDS1* gene is located approximately 240 kb upstream of Evi1, and MDS1/Evi1 is generated from the in-frame splicing of MDS1 to the second exon of Evi1.[36,43] Real-time PCR analysis demonstrated that the expression levels of MDS1/Evi1 were low and were not significantly increased when compared with controls (data not shown). The integration sites of *Evi1* were focused on two regions (Table 1). One is 15 kb upstream of start site of *Evi1* (mouse IDs 12, 14, 15), and another is 107 kb upstream of start site of *Evi1* (mouse IDs 4, 6, 7, 26). Morishita et al reported that the retrovirus integrations had occurred near or in 5′ noncoding exons of *Evi1* gene.[31] The integration site at 15 kb upstream of the start site of *Evi1* that we found is near to the site they reported.

In vivo collaboration between *Evi1* and AML1-D171N

Next, we tested to see if *Evi1* expression collaborates with AML1-D171N in inducing leukemia in the BMT model. Cotransduction of AML1-D171N and Evi1 into BM cells resulted in rapid induction of the disease in the mice that underwent transplantation that was essentially identical with the disease that developed after a long latency in the mice/D171N (Figures 1E,5). In fact, all the mice displayed increased number of blasts in the PB within a month after the transplantation of BM cells transduced with Evi1/D171N. Southern blot analysis showed that these leukemic cells were polyclonal (Figure 7B). These results indicate that AML1-D171N and Evi1 collaborate to induce MDS/AML with a distinct phenotype. On the other hand, cotransduction of AML1-S291fs and *Evi1* into BM cells did not induce MDS/AML in 5 months (data not shown). In the present work, mice that received transplants of BM cell–transduced *Evi1* alone did not present any abnormalities in 5 months (Figure 1E).

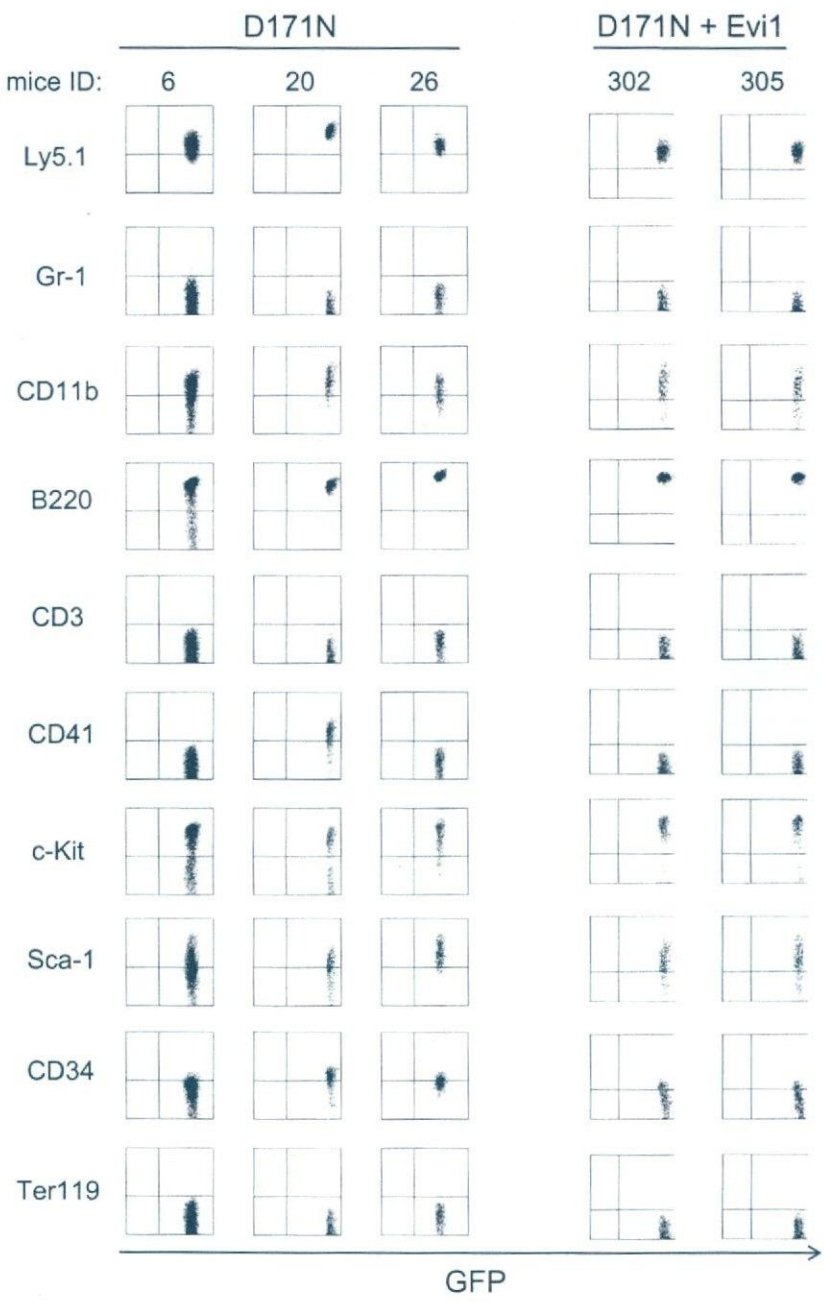

Figure 5. AML1-D171N induced a biphenotypic leukemia in concert with Evi1 in the BMT model. The dot plots show Ly5.1, Gr-1, CD11b, B220, CD3, CD41, c-kit, Sca-1, CD34, or Ter119 labeled with a corresponding PE-conjugated mAb versus expression of GFP. BM cells of morbid mice/D171N with high expression of *Evi1* (mouse IDs 6, 20, and 26) and those of morbid mice/D171N + *Evi1* (mouse IDs 302 and 305) displayed a similar pattern of surface markers, $CD11b^+$ and $B220^+$.

AML1-S291fs induced erythroid dysplasia with pancytopenia

In contrast to mice/D171N, most of mice/S291fs displayed remarkable erythroid dysplasia with continuous pancytopenia (Figures 3A-C,4A). A total of 2 of 8 mice/S291fs died of MDS-RAEB in which the percentage of blasts in the bone marrow was less than 20%, and 5 mice/S291fs developed MDS/AML. The mice displayed severe anemia but not leukocytosis in the PB, and the numbers of blasts were generally lower than those of MDS/AML mice transduced with AML1-D171N (Table S2). Surface markers of leukemic cells derived from mice/S291fs were different from those of mice/D171N (Figure S3).

We found integrations of the retrovirus in the intron of MN1 in 3 of 8 mice/S291fs (Table 1; mouse IDs 55, 56, and 58), and MN1 was overexpressed in the leukemic cells of these mice (Figure S2). The integration site was identical among these leukemic cells, indicating that leukemic cells of the 3 mice were derived from a single hematopoietic progenitor and that overexpression of MN1 induced expansion of the transduced stem cells during the 3-day culture period before the transplantation. Indeed, the mice with the integration at that MN1 site developed MDS/AML with shorter latencies (Table S2).

Discussion

We have established a mouse BMT model for MDS and MDS/AML using *AML1* mutants derived from patients with MDS,

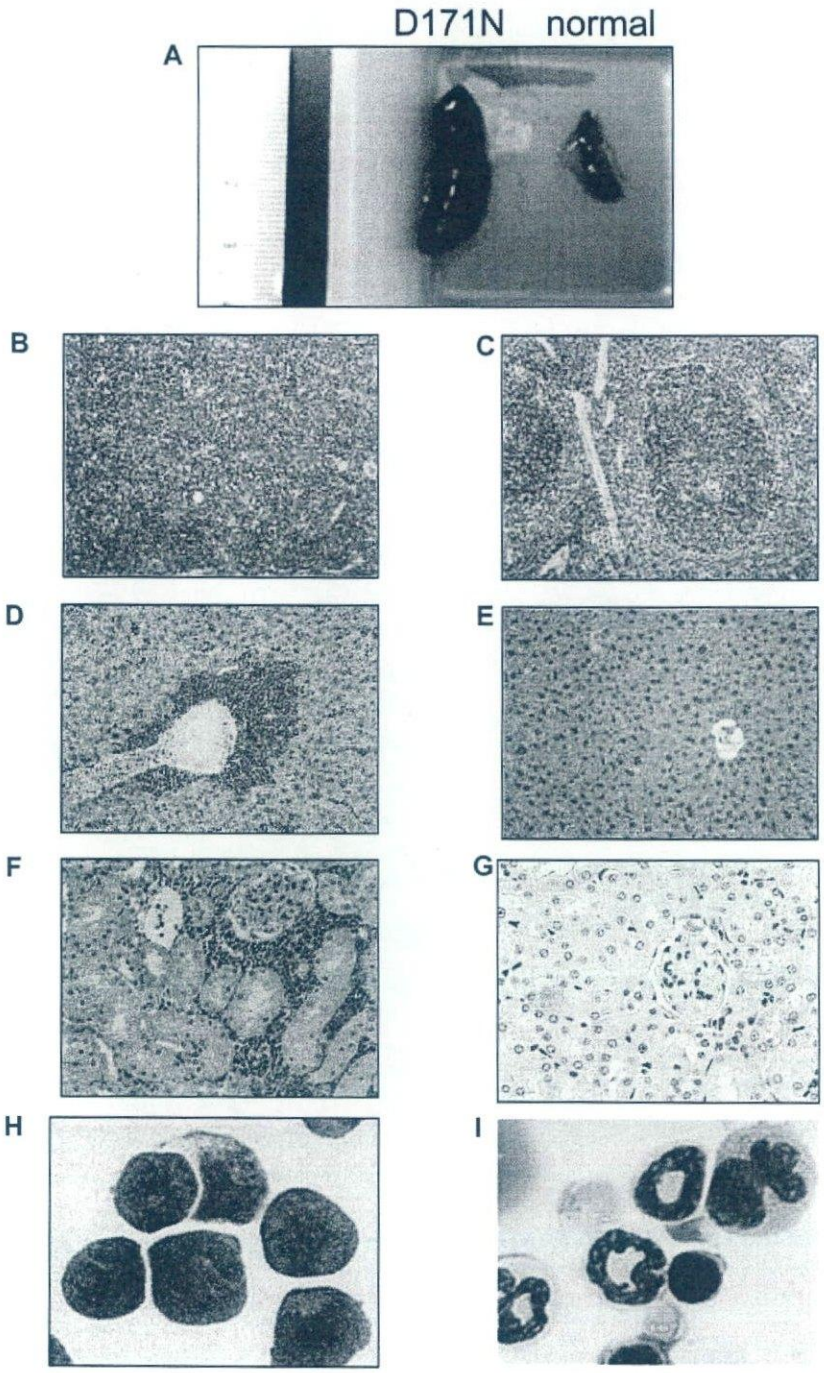

Figure 6. Leukemic cells of mice/D171N with high expression of Evi1 invaded into liver and kidney. (A) Spleen from morbid mice/D171N (left) and from normal mice (right). Histopathologic findings of (B) spleen, (D) liver, and (F) kidney infiltrated with leukemic cells from mice/D171N, stained with H&E. Histopathologic findings of (C) spleen, (E) liver, and (G) kidney from normal mice, stained with H&E. (H) Mice/D171N showed a high percentage of blasts in bone marrow. Cytospin preparations of BM cells from (H) mice/D171N and (I) normal mice, stained with Giemsa. (BX51 microscope, DP12 camera module; objective lens, UPlanFl; magnification, ×200 (B-E); ×100 (F,G); and ×1000 (H,I).

although previous studies either using similar BMT models or knock-in mice of *AML1* mutants failed to do so. There are several potential explanations for this discrepancy. First, because most *AML1* mutants work as dominant-negative forms, high expression levels of the mutants would be critical to effectively inhibit WT *AML1*. In this aspect, our BMT model has an advantage, using the efficient retrovirus vector pMYs[40] designed to achieve high expression in hematopoietic progenitor cells and, unlike most other retrovirus vectors, harbors splice donor and acceptor sites derived from the MFG vector to increase expression levels.[40,47] Second, using the efficient packaging cell line Plat-E,[39] we achieved high titers of retroviruses (average: 10^7 infection U/mL), which could result in the higher numbers of retrovirus integrations. This also increases the probabilities of up-regulating or disrupting important genes that collaborate with *AML1* mutants in inducing MDS and/or MDS/AML. Alternatively, it is also possible that the positions of *AML1* mutations are critical for the biological effect. We believe that the combination of these factors has put our system into practice.

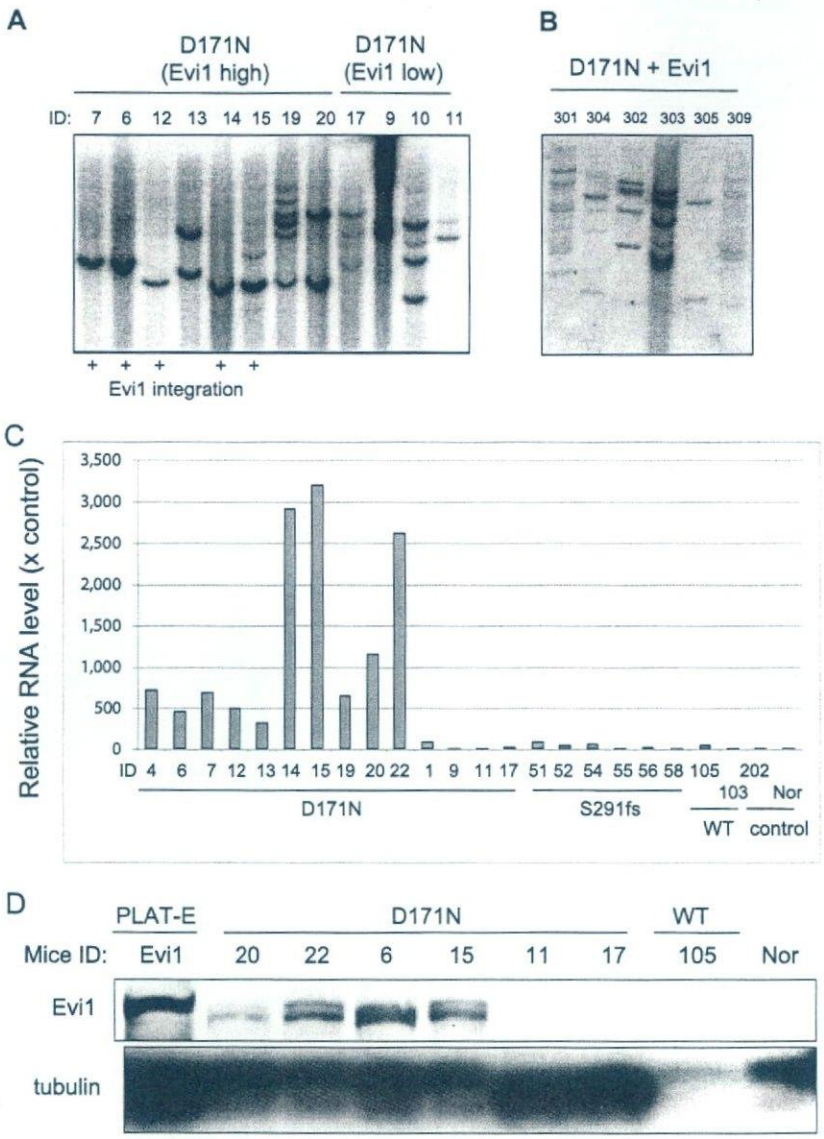

Figure 7. The mice/D171N with integration near *Evi1* site were monoclonal. (A) Southern blot analysis of mice/D171N. DNA samples were digested with *Eco*RI, which cut the retrovirus only once within the multicloning site. Probes used were DNA fragments of the GFP coding sequence. Mouse IDs are shown at the top of the panel. (B) The mice/D171N + *Evi1* were polyclonal. DNA samples were digested with *Eco*RI. Proviruses were probed with a GFP probe. (C) Real-time PCR for *Evi1* in BM derived from morbid mice/D171N or mice/S291fs or mice/WT or mice/mock. In addition to 6 samples from mice/D171N harboring integration near *Evi1* (mouse IDs 4, 6, 7, 12, 14, and 15), 4 samples derived from mice/D171N without integration near *Evi1* display high expression levels of Evi1 (mouse IDs 13, 19, 20, and 22). RNA from normal BM cells served as a control (RNA level = 1). (D) Western blot of lysates from spleen cells of mice/D171N, mice/WT, and normal mice and PLAT-E as controls. Samples from mice/D171N confirmed high expression of *Evi1* by RT-PCR showed expression of the protein (mouse IDs 6, 15, 20, and 22), but the other mice without high expression of *Evi1* by RT-PCR did not express the protein (mouse IDs 11, 17, and 105).

In the present MDS model, we used 2 *AML1* mutants, D171N and S291fsX300. The latter, a C-terminal–truncated form, is more potent as a dominant-negative form than the former, which harbors a point mutation in the RHD.[25,26] In this context, it is reasonable that the S291fs mutant induced the disease in the mice that underwent transplantation with a higher penetrance (Figure 1D). More important, expression of these mutants induced MDS/AML of distinct phenotypes in the mice that underwent transplantation: AML1-S291fs induced pancytopenia associated with dysplasia in the erythroid lineage, while AML1-D171N frequently induced hepatoslenomegaly and leukocytosis associated with marked myeloid dysplasia. This suggests that even different mutations of the same gene could induce heterogeneous diseases. As previously described,[25,26] AML1-D171N lost DNA-binding ability and hence transactivation potential because it possessed a point mutation in RHD essential for DNA-binding, while AML1-S291fs had increased DNA-binding ability but lost transactivation potential because it had an intact RHD but lacked a C-terminal transactivation domain. Thus, the different biological outcomes induced by *AML1* mutants could be explained in part by structural and functional differences between the mutants. In addition to the dominant-negative functions, these mutants may also have gain of function; the fact that AML1-KO mice did not develop leukemia[18] indicates that deletion of *AML1* alone is not sufficient to induce leukemia, suggesting the possibility that the *AML1* mutants have gain of function as well. Because *AML1* associates and forms a ternary complex with other transcriptional factors and cofactors via its specific domains, it is possible that these mutants exert different effects on the proliferation and differentiation of BM cells in the various contexts.

In BMT models using retrovirus-mediated gene transfer, the genes near the retrovirus integration sites are thought to affect the outcomes.[30-38] This sometimes obscures the significance of the transduced gene, but simultaneously will give us clues to understanding the collaboration of multiple genes in the development of leukemias. One of the intriguing findings of the present work is that high expression of *Evi1*, either caused by virus integration or by unknown mechanisms, was able to collaborate with AML1-D171N in inducing the homogeneous disease characterized by leukocytosis, severe myelodysplasia, and marked hepatosplenomegaly that

Table 1. Analysis of integration site

Mutant	Mouse ID	Count of Southern blot bands	Nearest gene	Chromosome no.	Gene ID	Distance to gene (start or end), bp	Location	Forward or reverse orientation	RTCGD hits
Experiment 1									
D171N	1	ND	*2010111I01Rik*	13	72061	238 927	Intron 10	F	0
D171N	1		*LOC100040862*	12	100040862	40 051	5′	F	0
D171N	4	ND	*Evil*	3	14013	107 412	5′	R	24
D171N	4		*Nsmce2*	15	68501	221 183	Intron 5	R	2
Experiment 2									
D171N	5	3	*Rreb1*	13	68750	14 071	5′	R	9
D171N	5		*LOC619665*	6	619665	123 854	5′	F	0
D171N	6	1	*Evil*	3	14013	106 286	5′	R	24
D171N	7	1	*Evil*	3	14013	106 286	5′	R	24
Experiment 3									
D171N	10	4	*B4galt6*	18	56386	8 961	Intron 1	R	0
D171N	11	2	*Rp1h*	1	19888	65 523	5′	F	0
Experiment 4									
D171N	12	1	*Evil*	3	14013	14 909	5′	F	24
D171N	13	2	*Slc38a2*	15	67760	41 018	5′	F	6
D171N	14	1	*Evil*	3	14013	15 002	5′	F	24
D171N	15	2	*Evil*	3	14013	14 850	5′	F	24
D171N	15		*Slc38a2*	15	22462	11 988	5′	R	6
S291fsX300	51	ND	*LOC100042800*	13	100042800	27 734	5′	R	0
S291fsX300	52	2	*P2rx7*	5	18439	40 672	intron 13	R	1
S291fsX300	52		*Gm pr2*	14	105446	17	intron 1	R	0
S291fsX300	54	2	*M srb3*	10	320183	98 981	3′	F	0
Empty	203	ND	*Dph5*	3	13609	70 064	5′	R	1
Experiment 5									
D171N	19	6	*Gch1*	14	14528	16 958	Intron 1	R	0
D171N	20	2	*Gch1*	14	14528	16 958	Intron 1	R	0
S291fsX300	55	2	*Mn1*	5	433938	16 024	Intron 1	F	8
S291fsX300	56	1	*Mn1*	5	433938	16 024	Intron 1	F	8
S291fsX300	58	1	*Mn1*	5	433938	16 024	Intron 1	F	8
Experiment 6									
D171N	22	ND	*Lrrc8c*	5	100604	16 056	5′	F	4
Experiment 7									
D171N	26	1	*Evil*	3	14013	106 710	5′	F	24
S291fsX300	60	3	*Dock10*	1	210293	163 158	Intron 1	R	0

RTGCD, Retroviral Tagged Cancer Gene Database[37]; and ND, not determined.

always developed to overt leukemia with high percentages of $B220^+$ and $CD11b^+$ blasts. Together with the recent findings that Evi1 expression was observed in patients with MDS and AML,[36,48] and that Evi1 alone did not induce AML in mouse models,[14,34,49,50] our result strongly suggested that AML1-D171N collaborated with Evi1 in inducing MDS/AML. It is interesting to note that AML1-S291fs never collaborated with *Evi1* during our examination (Table 1), again suggesting that these 2 *AML1* mutations transform hematopoietic cells through distinct mechanisms. Importantly, we confirmed the collaboration between AML1-D171N and *Evi1* in an in vivo experiment. Cotransduction of AML1-D171N and *Evi1* into BM cells resulted in rapid induction of MDS/AML in the mice that received transplants. In addition, the leukemic cells in most of these mice included more clones than those in mice/D171N (Figure 7B), indicating cooperation of *Evi1* and AML1-D171N. However, leukemic cells from one mouse (ID 305) seemed to be monoclonal and to contribute to oligoclonal leukemia of mouse 304. In addition, it took 2 to 3 months for leukemias induced by the combination of AML1-D171N and Evi1 to kill the mice that received transplants. Together, these result suggested that while AML1-D171N and Evi1 overexpression collaborated in inducing leukemia, additional steps were required for efficient transformation of hematopoietic progenitors. In the absence of Evi1 high expression, AML1-D171N caused MDS or MDS/AML with low percentages of blasts in BM but still with hepatosplenomegaly. This indicates that hepatosplenomegaly had something to do with AML1-D171N.

In contrast to mice/D171N, most mice/S291fs succumbed to either MDS-RAEB with fatal severe anemia following continuous pancytopenia or MDS/AML without leukocytosis. The integration site in the intron 1 of the *MN1* gene found in leukemic cells of 3 mice was derived from the same cell. We also found that *MN1* was overexpressed in the leukemic cells of these mice, suggesting that overexpression of *MN1* induced effective expansion of leukemic stem cells. Recently, Heuser et al reported that high expression of *MN1* correlated with poor outcome in AML with normal cytogenetics.[51] Moreover, Slape et al identified *MN1* as potential collaborators of NUP98/HOXD13 to induce leukemia.[42] Further work will be required to investigate the role of MN1 in MDS/AML.

One fundamental question of this study was whether *AML1* mutants alone induce MDS and MDS/AML. In our experiments, 5 of the 6 surviving mice/D171N showed a disappearance of GFP^+ cells in time, suggesting that AML1-D171N alone was not able to induce MDS/AML. Previous studies using gene-engineered mice and a BMT model demonstrated that *AML1*

fusions caused by chromosomal translocations alone were insufficient to induce AML,[7-12] except for *AML1-MDS1-Evi1*, which by itself induced AML with a long latency.[52] In addition, several lines of evidence[30-38] that implicated the integration site of retroviruses for different biological outcomes led us to consider the same possibility in this BMT model. Indeed, we identified frequent retrovirus integrations near the *Evi1* gene in the BM cells derived from mice/D171N whose leukemic cells displayed nearly identical phenotypes and concomitant elevated expression of *Evi1*. Importantly, coexpression of AML1-D171N and *Evi1* induced the same leukemia with shorther latencies, demonstrating the collaboration between AML1-D171N and *Evi1* in vivo. These results showed the power of in vivo insertional mutagenesis of retroviruses in a search for genes involved in the pathogenesis of MDS and MDS/AML.

Finally, it is important to relate these in vivo results to clinical data of the human disease. The recent finding[25-27] that *AML1* point mutations in the C-terminal regions were almost exclusively found in MDS-RAEB and MDS/AML, but not in de novo AML, coincided with our data that AML1-S291fs tended to induce MDS-RAEB–like symptoms in this BMT model. Clinical findings[25-27] that the RHD point mutation was often found in de novo AML, mainly AML M0, in addition to MDS-RAEB and MDS/AML, was also in accordance with our data that AML1-D171N induced more progressive MDS/AML with higher percentages of blasts when compared with AML1-S291fs. Classification of MDS and MDS/AML is always controversial because of the heterogeneity of the disease.[1,2,27] In the future, this disease will be reclassified based on genetic alterations and their combinations.

In summary, we have generated a mouse BMT model of MDS-RAEB and MDS/AML. The current BMT model, mimicking AML1-related MDS, will be useful for understanding molecular pathogenesis and establishing new therapeutic strategy for MDS and MDS/AML.

Acknowledgments

We greatly thank Dr Mineo Kurokawa for kindly providing the anti-*Evi1* antibody and Dr Takuro Nakamura and Dr Kazuhiro Morishita for kindly providing pMYs-*Evi1*-IG. We also thank Dr Christopher Slape for kindly giving information about the condition of RT-PCR for MN1. We are grateful to Dr Dovie Wylie for excellent language assistance. We thank Yumi Fukuchi, Fumi Shibata, Miyuki Ito, and Ai Hishiya for technical assistance.

This work was supported by the Grant-in-aid for Cancer Research supported by the Ministry of Health, Labor and Welfare, Japan; a grant from the Vehicle Racing Commemorative Foundation; and a grant from the Japan Society for the Promotion of Science (JSPS). N.W.-O. is a JSPS research fellow.

Authorship

Contributions: N.W.O. did all the experiments and participated in writing the manuscript; J.K. oversaw all the experiments and actively participated in manuscript writing; R.O. provided experimental guidance about and assisted in the BMT model; H.H. provided the general information and made the constructs of AML1 mutants; Y.H. made the constructs of AML1 mutants; Y.K. assisted in the experiments of BMT model; H.N. provided experimental guidance about cell sorting and staining; T.N. provided experimental guidance of the BMT model; T.I. provided the general information and constructs of AML1 mutants; and T.K. conceived and directed the project, secured funding, and actively participated in manuscript writing.

Conflict-of-interest disclosure: The authors declare no competing financial interests.

Correspondence: Toshio Kitamura, Division of Cellular Therapy, Advanced Clinical Research Center, The Institute of Medical Science, The University of Tokyo, 4-6-1 Shirokanedai, Minato-ku, Tokyo 108-8639, Japan; e-mail: kitamura@ims.u-tokyo.ac.jp.

References

1. Mufti G, List AF, Gore SD, Ho AY. Myelodysplastic syndrome. Am Soc Hematol Educ Program. 2003;176-199.
2. Heaney ML, Golde DW. Myelodysplasia. N Engl J Med. 1999;340:1649-1660.
3. Legare RD, Gilliland DG. Myelodysplastic syndrome. Curr Opin Hematol. 1995;2:283-292.
4. Hirai H, Kobayashi Y, Mano H, et al. A point mutation at codon 13 of the N-ras oncogene in myelodysplastic syndrome. Nature. 1987;327:430-432.
5. Hirai H, Okada M, Mizoguchi H, et al. Relationship between an activated N-ras oncogene and chromosomal abnormality during leukemic progression myelodysplastic syndrome. Blood. 1988; 71:256-258.
6. Gilliland DG, Griffin JD. Role of FLT3 in leukemia. Curr Opin Hematol. 2002;9:274-281.
7. Schessl C, Rawat VP, Cusan M, et al. The AML1-ETO fusion gene and the FLT3 length mutation collaborate in inducing acute leukemia in mice. J Clin Invest. 2005;115:2159-2168.
8. Okuda T, Cai Z, Yang S, et al. Expression of a knocked-in AML1-ETO leukemia gene inhibits the establishment of normal definitive hematopoiesis and directly generates dysplastic hematopoietic progenitors. Blood. 1998;91:3134-3143.
9. Rhoades KL, Hetherington CJ, Harakawa N, et al. Analysis of the role of AML1-ETO in leukemogenesis, using an inducible transgenic mouse model. Blood. 2000;96:2108-2115.
10. Higuchi M, O'Brien D, Kumaravelu P, Lenny N, Yeoh EJ, Downing JR. Expression of a conditional AML1-ETO oncogene bypasses embryonic lethality and establishes a murine model of human t(8;21) acute myeloid leukemia. Cancer Cell. 2002;1:63-74.
11. Fenske TS, Pengue G, Mathews V, et al. Stem cell expression of the AML1/ETO fusion protein induces a myeloproliferative disorder in mice. Proc Natl Acad Sci U S A. 2004;101:15184-15189.
12. de Guzman CG, Warren AJ, Zhang Z, et al. Hematopoietic stem cell expansion and distinct myeloid developmental abnormalities in a murine model of the AML1-ETO translocation. Mol Cell Biol. 2002;22:5506-5517.
13. Ono R, Nakajima H, Ozaki K, et al. Dimerization of MLL fusion proteins and FLT3 activation synergize to induce multiple-lineage leukemogenesis. J Clin Invest. 2005;115:919-929.
14. Buonamici S, Li D, Chi Y, et al. EVI1 induces myelodysplastic syndrome in mice. J Clin Invest. 2004;114:713-719.
15. Lin YW, Slape C, Zhang Z, Aplan PD. NUP98-HOXD13 transgenic mice develop a highly penetrant, severe myelodysplastic syndrome that progresses to acute leukemia. Blood. 2005;106: 287-295.
16. Okuda T, van Deursen J, Hiebert SW, Grosveld G, Downing JR. AML1, the target of multiple chromosomal translocations in human leukemia, is essential for normal fetal liver hematopoiesis. Cell. 1996;84:321-330.
17. Wang Q, Stacy T, Binder M, et al. Disruption of the Cbfa2 gene causes necrosis and hematorrhaging in the central nervous system and blocks definitive hematopoiesis. Proc Natl Acad Sci U S A. 1996;93:3444-3449.
18. Ichikawa M, Asai T, Saito T, et al. AML-1 is required for megakaryocytic maturation and lymphocytic differentiation, but not for maintenance of hematopoietic stem cells in adult hematopoiesis. Nat Med. 2004;10:299-304.
19. Song WJ, Sullivan MG, Legare RD, et al. Haploinsufficiency of CBFA2 causes familial thrombocytopenia with propensity to develop acute myelogenous leukaemia. Nat Genet. 1999;23:166-175.
20. Michaud J, Wu F, Osato M, et al. In vitro analyses of known and novel RUNX1/AML1 mutations in dominant familial platelet disorder with predisposition to acute myelogenous leukemia: implications for mechanisms of pathogenesis. Blood. 2002;99:1364-1372.
21. Osato M, Asou N, Abdalla E, et al. Biallelic and heterozygous point mutations in the runt domain of the AML1/PEBP2alphaB gene associated with myeloblastic leukemias. Blood. 1999;93:1817-1824.
22. Preudhomme C, Warot-Loze D, Roumier C, et al. High incidence of biallelic point mutations in the Runt domain of the AML1/PEBP2alpha B gene in

Mo acute myeloid leukemia and in myeloid malignancies with acquired trisomy 21. Blood. 2000; 96:2862-2869.

23. Imai Y, Kurokawa M, Izutsu K, et al. Mutations of the AML1 gene in myelodysplastic syndrome and their functional implications in leukemogenesis. Blood. 2000;96:3154-3160.
24. Langabeer SE, Gale RE, Rollinson SJ, Morgan GJ, Linch DC. Mutations of the AML1 gene in acute myeloid leukemia of FAB types M0 and M7. Genes Chromosomes Cancer. 2002;34:24-32.
25. Harada H, Harada Y, Tanaka H, Kimura A, Inaba T. Implications of somatic mutations in the AML1 gene in radiation-associated and therapy-related myelodysplastic syndrome/acute myeloid leukemia. Blood. 2003;101:673-680.
26. Harada H, Harada Y, Niimi H, Kyo T, Kimura A, Inaba T. High incidence of somatic mutations in the AML1/RUNX1 gene in myelodysplastic syndrome and low blast percentage myeloid leukemia with myelodysplasia. Blood. 2004;103:2316-2324.
27. Osato M. Point mutations in the RUNX1/AML1 gene: another actor in RUNX leukemia. Oncogene. 2004;23:4284-4296.
28. Steensma DP, Gibbons RJ, Mesa RA, Tefferi A, Higgs DR. Somatic point mutations in RUNX1/CBFA2/AML1 are common in high-risk myelodysplastic syndrome, but not in myelofibrosis with myeloid metaplasia. Eur J Haematol. 2005;74:47-53.
29. Christiansen DH, Andersen MK, Pedersen-Bjergaard J. Mutations of AML1 are common in therapy-related myelodysplasia following therapy with alkylating agents and are significantly associated with deletion or loss of chromosome arm 7q and with subsequent leukemic transformation. Blood. 2004;104:1474-1481.
30. Yamashita N, Osato M, Huang L, et al. Haploinsufficiency of Runx1/AML1 promotes myeloid features and leukaemogenesis in BXH2 mice. Br J Haematol. 2005;131:495-507.
31. Morishita K, Parker DS, Mucenski ML, Jenkins NA, Copeland NG, Ihle JN. Retroviral activation of a novel gene encoding a zinc finger protein in IL-3-dependent myeloid leukemia cell lines. Cell. 1988;54:831-840.
32. Mucenski ML, Taylor BA, Ihle JN, et al. Identification of a common ecotropic viral integration site, Evi1, in the DNA of AKXD murine myeloid tumors. Mol Cell Biol. 1988;8:301-308.
33. Calmels B, Ferguson C, Laukkanen MO, et al. Recurrent retroviral vector integration at the Mds1/Evi1 locus in nonhuman primate hematopoietic cells. Blood. 2005;106:2530-2533.
34. Kustikova O, Fehse B, Modlich U, et al. Clonal dominance of hematopoietic stem cells triggered by retroviral gene marking. Science. 2005;308: 1171-1174.
35. Modlich U, Kustikkova OS, Schmidt M, et al. Leukemias following retroviral transfer of multidrug resistance 1 (MDR1) are driven by combinatorial insertional mutagenesis. Blood 2005;105:4235-4246.
36. Nucifora G, Laricchia-Robbio L, Senyuk V. Evi1 and hematopoietic disorders: history and perspectives. Gene. 2006;368:1-11.
37. Akagi K, Suzuki T, Stephens RM, Jenkins NA, Copeland NG. RTCGD: retroviral tagged cancer gene database. Nucleic Acids Res. 2004;32:523-527.
38. Jin G, Yamazaki Y, Takuwa M, et al. Trib1 and Evi1 cooperate with Hoxa and Meis1 in myeloid leukemogenesis. Blood. 2007;109:3998-4005.
39. Morita S, Kojima T, Kitamura T. Plat-E: an efficient and stable system for transient packaging of retroviruses. Gene Ther. 2000;7:1063-1066.
40. Kitamura T, Koshino Y, Shibata F, et al. 2003. Retrovirus-mediated gene transfer and expression cloning: powerful tools in functional genomics. Exp. Hematol. 2003;31:1007-1014.
41. Kogan SC, Ward JM, Anver MR, et al. Bethesda proposals for classification of nonlymphoid hematopoietic neoplasms in mice. Blood. 2002;100: 238-245.
42. Slape C, Hartung H, Lin YW, et al. Retroviral insertional mutagenesis identifies genes that collaborate with NUP98-HOXD13 during leukemic transformation. Cancer Res. 2007;67:5148-55.
43. Wimmer K, Vinatzer U, Zwirn P, et al. Comparative expression analysis of the antagonistic transcription factors EVI1 and MDS1-EVI1 in murine tissues and during in vitro hematopoietic differentiation. Biochem Biophys Res Commun. 1998; 252:691-6.
44. Riley J, Butler R, Ogilvie D, et al. A novel, rapid method for the isolation of terminal sequences from yeast artificial chromosome (YAC) clones. Nucl. Acids Res. 1990;18:2887-2890.
45. Arnold C, Hodgson IJ. Vectorette PCR: a novel approach to genome walking. PCR Methods Appl. 1991;1:39-42.
46. Tsuzuki S, Hong D, Gupta R, Matsuo K, Seto M, Enver T. Isoform-specific potentiation of stem and progenitor cell engraftment by AML1/RUNX1. PLoS Med. 2007;4:e172.
47. Riviere I, Brose K, Mulligan RC. Effects of retroviral vector design on expression of human adenosine deaminase in murine bone marrow transplant recipients engrafted with genetically modified cells. Proc Natl Acad Sci U S A. 1995; 92:6733-6737.
48. Langabeer SE, Rogers JR, Harrison G, et al. EVI1 expression in acute myeloid leukaemia. Br J Haematol. 2001;112:208-211.
49. Cuenco GM, Ren R. Both AML1 and EVI1 oncogenic components are required for the cooperation of AML1/MDS1/EVI1 with BCR/ABL in the induction of acute myelogenous leukemia in mice. Oncogene. 2004;23:569-579.
50. Louz D, van den Broek M, Verbakel S, et al. Erythroid defects and increased retrovirally-induced tumor formation in Evi1 transgenic mice. Leukemia. 2000;14:1876-1884.
51. Heuser M, Beutel G, Krauter J, et al. High meningioma 1 (MN1) expression as a predictor for poor outcome in acute myeloid leukemia with normal cytogenetics. Blood. 2006;108:3898-905.
52. Cuenco GM, Nucifora G, Ren R. Human AML1/MDS1/EVI1 fusion protein induces an acute myelogenous leukemia (AML) in mice: a model for human AML. Proc Natl Acad Sci USA. 2000;97: 1760-1765.

Analysis of mouse LMIR5/CLM-7 as an activating receptor: differential regulation of LMIR5/CLM-7 in mouse versus human cells

Yoshinori Yamanishi,[1] Jiro Kitaura,[1] Kumi Izawa,[1] Takayuki Matsuoka,[1] Toshihiko Oki,[1] Yang Lu,[1] Fumi Shibata,[1] Satoshi Yamazaki,[2] Hidetoshi Kumagai,[1] Hideaki Nakajima,[1] Mari Maeda-Yamamoto,[3] Victor L. J. Tybulewicz,[4] Toshiyuki Takai,[5] and Toshio Kitamura[1]

[1]Division of Cellular Therapy, Advanced Clinical Research Center, Institute of Medical Science, University of Tokyo, Tokyo, Japan; [2]Laboratory of Stem Cell Therapy, Center for Experimental Medicine, Institute of Medical Science, University of Tokyo, Tokyo, Japan; [3]National Institute of Vegetable and Tea Science, National Agriculture Research Organization, Shizuoka, Japan; [4]Division of Immune Cell Biology, National Institute for Medical Research, London, United Kingdom; and [5]Department of Experimental Immunology, Institute of Development, Aging and Cancer, Tohoku University, Sendai, Japan

We have analyzed leukocyte mono-Ig–like receptor 5 (LMIR5) as an activating receptor among paired LMIRs. Mouse LMIR5 (mLMIR5) is expressed in myeloid cells such as mast cells, granulocytes, macrophages, and dendritic cells. Cross-linking of transduced mLMIR5 in bone marrow–derived mast cells (BMMCs) caused activation events, including cytokine production, cell survival, degranulation, and adhesion to the extracellular matrix. mLMIR5 associated with DAP12 and to a lesser extent with DAP10, and mLMIR5-mediated functions of BMMCs were strongly inhibited by DAP12 deficiency. Importantly, cross-linking of endogenous mLMIR5 induced Syk-dependent activation of fetal liver–derived mast cells. Unlike mLMIR5, cross-linking of human LMIR5 (hLMIR5) induced cytokine production of BMMCs even in the absence of both DAP12 and DAP10, suggesting the existence of unidentified adaptors. Interestingly, hLMIR5 possessed a tyrosine residue (Y188) in the cytoplasmic region. Signaling via Y188 phosphorylation played a predominant role in hLMIR5-mediated cytokine production in DAP12-deficient, but not wild-type BMMCs. In addition, experiments using DAP10/DAP12 double-deficient BMMCs suggested the existence of Y188 phoshorylation-dependent and -independent signals from unidentified adaptors. Collectively, although both mouse and human LMIR5 play activatory roles in innate immunity cells, the functions of LMIR5 were differentially regulated in mouse versus human cells. (Blood. 2008;111:688-698)

Introduction

It is widely accepted that mast cells are major effector cells in allergic inflammation through a high-affinity IgE receptor (FcεRI). However, recent advances have delineated the significant roles of mast cells in both innate and adaptive immune responses.[1-4]

To find a novel immune receptor expressed on mast cells, we previously performed a signal sequence trap based on retrovirus-mediated expression screening (SST-REX).[5] In this screening, we isolated a cDNA for a novel immune receptor, leukocyte mono-Ig–like receptor 1 (LMIR1),[6] using cDNA library of bone marrow–derived mast cells (BMMCs). Successively, other members of the LMIR family were cloned by searching for sequences homologous with the Ig-like domain of LMIR1. We and others have demonstrated that LMIR1/CMRF-35–like Ig-like molecule-8 (CLM-8)/myeloid-associated Ig-like receptor-I (MAIR-I)/CD300a and LMIR2/CLM-4/MAIR-II/dendritic cell–derived Ig-like receptor 1 (DIgR1)/CD300d as well as LMIR3/CLM-1 and LMIR4/CLM-5 were a pair of inhibitory and activating, respectively, receptors with high homology in the Ig-like domain.[6-14] LMIR/CLM forms a family of paired receptors mainly expressed in myeloid cells.[6-14] In general, activating receptors do not contain any signaling motifs in the short cytoplasmic tails, but transmit signals by associating with immunoreceptor tyrosine–based activation motif (ITAM) or the related activating motif-bearing molecules via a positively charged residue in the transmembrane domain.[15-19] In the present study, we cloned a cDNA for mouse LMIR5 (mLMIR5)/CLM-7 from a BMMC cDNA library. Analysis of DAP10-, DAP12-, and FcRγ-deficient BMMCs demonstrated the predominant role of DAP12 in the activating functions of mLMIR5.

Structural differences in immune receptors in mouse versus human cells sometimes result in differing immunologic responses. For example, human NKG2D associates only with DAP10. On the other hand, mouse NKG2D has 2 splice variants, where the long isoform (NKG2D-L) associates exclusively with DAP10 and the short isoform (NKG2D-S) associates with both DAP10 and DAP12.[20-23] Interestingly, human LMIR5 (hLMIR5)/CD300b/immune receptor expressed by myeloid cell-3 (IREM-3),[24] but not mLMIR5, contained a putative tyrosine phosphorylation motif (YXN) in its short cytoplasmic tail. The present results indicated that DAP12 plays a primary role in functions of mLMIR5, while both DAP12 and DAP10 play roles in functions of its human counterpart hLMIR5. Consistent with a recent report by Martinez-Barriocanal and Sayos,[24] our results also implicated an unidentified adaptor in the hLMIR5-mediated signaling pathway, which was activated through phosphorylation of the tyrosine in the absence of DAP12. In addition, the experiment using DAP12-deficient and

Submitted April 16, 2007; accepted September 18, 2007. Prepublished online as *Blood* First Edition paper, October 10, 2007; DOI 10.1182/blood-2007-04-085787.

The online version of this article contains a data supplement.

The publication costs of this article were defrayed in part by page charge payment. Therefore, and solely to indicate this fact, this article is hereby marked "advertisement" in accordance with 18 USC section 1734.

DAP10/DAP12 double-deficient BMMCs revealed Y188 phosphorylation–dependent and –independent signals downstream of hLMIR5.

Methods

Cells

Murine cell lines used in this study were as follows: FDC-P1, J774-1, RAW264.7, M1, L-G, 32Dcl3, P815, MC/9, L8057, Ba/F3, WEHI231, A20, EL4, BW5147, and DC2.4. L8057 and DC2.4 were a kind gift from Dr Y. Hirabayashi (National Institute of Health Sciences, Tokyo, Japan) and Dr K. L. Rock (University of Massachusetts Medical School, Worcester, MA), respectively. Peripheral blood (PB) cells, bone marrow (BM) cells, splenocytes, thymocytes, and peritoneal cells derived from C57BL/6 mice (or CBA/J mice) were purified as described.[14] CBA/J mice or C57BL/6J mice (Charles River Laboratories Japan, Yokohama, Japan) were used at 8 to 10 weeks of age for isolation of tissues and cells. All procedures were approved by an institutional review committee. BMMCs or fetal liver mast cells (FLMCs) were generated and cultured as described.[25-27] BM-derived macrophage (BMMΦ), BM-derived myeloid dendritic cells (BMmDCs), and BM-derived plasmacytoid dendritic cells (BMpDCs) were cultured as described.[14] The following mutant mice were used: *DAP10*$^{-/-}$,[20] *DAP12*$^{-/-}$,[28] *FcRγ*$^{-/-}$,[29] and *Syk*$^{+/-}$.[30]

Antibodies and other reagents

Cytokines and anti-mLMIR5 polyclonal antibody (Ab) was obtained from R&D Systems (Minneapolis, MN). Fluorescein isothiocyanate (FITC)–conjugated anti–mouse B220, CD3, CD11b, and Gr-1 mAb were purchased from eBioscience (San Diego, CA). FITC-conjugated anti–mouse IgE, FITC-conjugated anti–mouse Ig polyclonal Ab, R-phycoerythrin (PE)–conjugated anti–mouse c-Kit mAb, and mouse antitrinitrophenyl (TNP) IgE (C38-2) were from BD Pharmingen (San Diego, CA). Anti–Flag mAb (M2), mouse IgG1 mAb (MOPC21), goat IgG polyclonal Ab, and mouse antidinitrophenyl (DNP) IgE mAb (SPE-7) were from Sigma-Aldrich (St Louis, MO). Donkey PE-conjugated F(ab')$_2$ anti–goat IgG Ab was from Jackson Immunoresearch Laboratories (West Grove, PA). Anti-Myc mAb (9E10) was from Roche Diagnostics (Indianapolis, IN). Rabbit anti–mouse DAP12 polyclonal Ab was a kind gift from Dr N. Aoki (Asahikawa Medical College, Asahikawa, Japan). Mouse antiphosphotyrosine mAb (4G10) was purchased from Upstate Biotechnology (Charlottesville, VA), and other phospho-specific Abs were from Cell Signaling Technology (Beverly, MA). Other Abs were from Santa Cruz Biotechnology (Santa Cruz, CA). Bovine serum fibronectin (FN), human plasma fibrinogen (FB), and N-glycosidase F were purchased from Sigma-Aldrich, Chemicon (Temecula, CA), and New England Biolabs (Beverly, MA), respectively.

Gene expression analysis

Expression of mLMIR5 was analyzed by reverse transcriptase–polymerase chain reaction (RT-PCR) as described.[14] Amplification of mLMIR5 as well as β-actin for normalization was performed with the following primers: 5′-TTACCATGGAGATGCTCAGG-3 (base: 266-285) and 5′-TCGCTACAGAGAGTGTGTCTCC-3′ (base: 590-569) for mLMIR5; and 5′-CATCACTATTGGCAACGAGC-3′ and 5′-ACGCAGCTCAGTAACAGTCC-3′ for β-actin. Relative expression levels of DAP10, DAP12, and FcRγ among samples were measured by real-time RT-PCR. cDNA was amplified using a LightCycler FastStart DNA Master SYBR Green I kit (Roche Diagnostics, Mannheim, Germany) under the following conditions: 1 cycle of 95°C for 10 seconds, 40 cycles of 95°C for 5 seconds, and 60°C for 20 seconds. All samples were independently analyzed 3 times. The following primers were used: 5′-CCCCCCAGGCTACCTCC-3′ and 5′-TGACATGACCGCATCTGCA-3′ for DAP10; 5′-CAAGATGCGACTGTTCTTCCG-3′ and 5′-GGTCTCTGACCCTGAAGCTCC-3′ for DAP12; 5′-GCCGTGATCTTGTTCTTGCTC-3′ and 5′-CTGCCTTTCGGACCTGGAT-3′ for FcRγ; and 5′-ATGTGTCCGTCGTGGATCTGA-3′ and 5′-TTGAAGTCGCAGGAGACAACC-3′ for GAPDH. Relative gene expression levels were calculated using standard curves generated by serial dilutions of cDNA and normalized by a GAPDH expression level. Product quality was checked by melting curve analysis via LightCycler software (Roche Diagnostics).

DNA constructs

The GenBank/European Molecular Biology Laboratory (EMBL[31])/DNA Data Bank of Japan (DDBJ[32]) database was searched by using the amino acid sequence of the Ig-like domain of mLMIR1. Based on the sequence data, cDNA of mouse and human LMIR5 were isolated by PCR from a cDNA library of BMMCs (derived from CBA/J or B57BL/6 mice) and a cDNA library of human peripheral mononuclear cells (PMCs), respectively, and confirmed by sequencing as described.[6] The cDNA fragment of mLMIR5 or hLMIR5, lacking the signal sequence, was tagged with an Flag or Myc epitope at the N terminus. The resultant Flag or Myc-mLMIR5 or hLMIR5 was subcloned into a pME18s vector containing a SLAM signal sequence (a gift from Hisashi Arase, Osaka University, Osaka, Japan)[33] to generate pME-Flag, Myc-mLMIR5, or hLMIR5. The resultant SLAM signal sequence-Flag, Myc-mLMIR5, or hLMIR5 was subcloned into a pMXs-IRES-puro^r (pMXs-IP)[34] retroviral vector to generate pMXs-Flag or Myc-mLMIR5 or hLMIR5-IP. Two-step PCR mutagenesis was performed in the replacement of K158 (lysine with a positive charge) of hLMIR5 with Q (glutamine with a neutral charge) and Y188 of hLMIR5 with F (phenylalanine).

Transfection and infection

Retroviral transfection was as described.[6,34] Briefly, retroviruses were generated by transient transfection of PLAT-E packaging cells[35] with FuGENE 6 (Roche Diagnostics). BM cells, BMMCs, or Ba/F3 cells were infected with retroviruses in the presence of 10 μg/mL polybrene. After 48 hours, cell selection was started with appropriate antibiotics.[34]

Flow cytometry

Cells were stained as described.[14] Flow cytometric analysis was performed with FACSCalibur (BD Biosciences, Mountain View, CA) equipped with CellQuest software and FlowJo software (Tree Star, Ashland, OR). For mLMIR5 staining, cells were incubated with 20 μg/mL anti-mLMIR5 polyclonal Ab or goat polyclonal IgG Ab as control, before incubation with 10 μg/mL PE-conjugated anti-goat IgG F(ab')$_2$ Ab.

Immunoprecipitation and Western blotting

Cells were lysed with NP-40 lysis buffer containing protease and phosphatase inhibitor cocktail (Sigma-Aldrich). Cell lysates were assayed using a protein assay kit (Bio-Rad, Hercules, CA). Immunoprecipitation and Western blotting were performed as described.[14]

Measurement of cytokines and histamines and adhesion assay

BMMCs and FLMCs were stimulated with either 20 μg/mL anti-mLMIR5 Ab, 20 μg/mL control IgG, or 100 nM phorbol-12-myristate13-acetate (PMA). BMMCs transduced with a Flag-tagged hLMIR5 were stimulated with 20 μg/mL anti-Flag mAb or 20 μg/mL control IgG. In some experiments, BMMCs sensitized with 1 μg/mL anti-TNP IgE for 12 hours were stimulated with 100 ng/mL TNP-BSA. TNF-α, IL-6, and MCP-1 concentrations in culture supernatants were measured using enzyme-linked immunosorbent assay (ELISA) kits (BD Pharmingen and R&D Systems). Histamine released during a 50-minute incubation period was measured as described.[25] Adhesion assay was described previously.[26]

Statistical analysis

Data are shown as means plus or minus standard deviation (SD), and statistical significance was determined by the Student *t* test with *P* levels less than .05 as statistically significant.

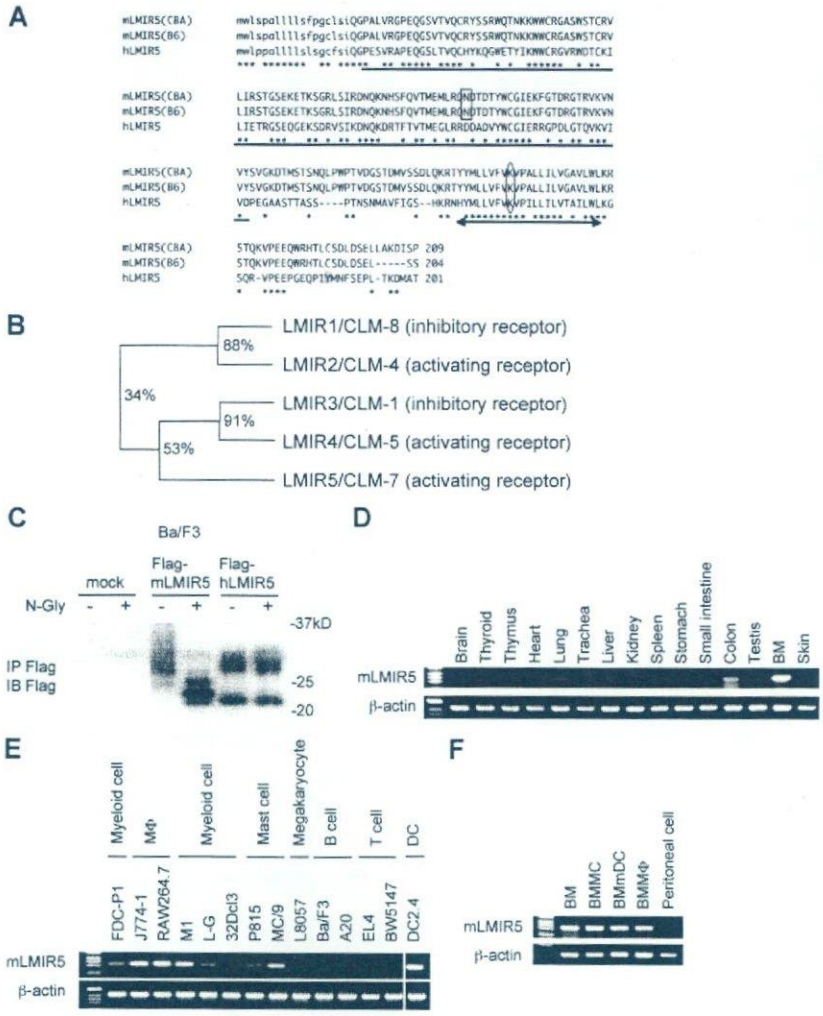

Figure 1. Molecular characteristics and gene expression of LMIR5. (A) Alignment of amino acid sequences for mLMIR5 and hLMIR5. CBA and B6 indicate CBA/J mice and C57BL/6 mice, respectively. *Identical amino acids in mLMIR5 and hLMIR5. The putative signal sequence is shown in lower case. The variable type Ig-like domain is underlined; the potential N-linked glycosylation site is boxed. The transmembrane domain is marked by an arrow; the positive-charged amino acid residue (lysine) in the transmembrane domain is circled. Y188 in the cytoplasmic tail of hLMIR5 is shaded. (B) The phylogenetic tree of LMIR1/2/3/4/5 is shown based on homology with the Ig-like domain. Percentage of identity in amino acid sequences of the Ig-like domain was indicated. (C) Lysates of Ba/F3 cells transduced with either a Flag-tagged mLMIR5, a Flag-tagged hLMIR5, or mock were immnoprecipitated with anti-Flag mAb. The precipitates treated with or without N-glycosidase F were immunoblotted with anti-Flag mAb. (D-F) RT-PCR analysis on mLMIR5 expression in murine tissues (D), hematopoietic cell lines (E), and primary hematopoietic cells (F). Specific primers were used for mLMIR5 or β-actin as control. Vertical lines have been inserted to indicate a repositioned gel lane.

Results

Structure of mLMIR5

To identify other members of LMIR besides LMIR1/2,[6] we searched the database from GenBank/EMBL/DDBJ by using the sequence encoding the Ig-like domain of LMIR1/CLM-8. Based on this, we identified and cloned mLMIR5/CLM-7 in addition to another pair, LMIR3/CLM-1 and LMIR4/CLM-5, from a BMMC cDNA library. An Ig-like domain of mLMIR5 shared 34% and 53% identity at amino acid sequences with that of LMIR1 and LMIR3, respectively (Figure 1A,B).[6] We also cloned its human ortholog from a human PMC cDNA library and found that hLMIR5 shared a 55% identity at overall amino acid sequences with mLMIR5 (Figure 1A). The sequence analysis revealed that mLMIR5 and hLMIR5 are identical to CLM-7[8,9] and IREM-3,[24] respectively. Because hLMIR5/IREM-3 has been recently characterized, we analyzed the structure and functions of mLMIR5/CLM-7 to compare them with those of hLMIR5/IREM-3. mLMIR5 was a type I transmembrane protein composed of an N-terminal signal peptide, an extracellular domain containing a single V-type Ig domain, a transmembrane domain with a positively charged amino acid (lysine), and a short cytoplasmic tail without any signaling motif (Figure 1A). mLMIR5 protein derived from CBA/J mice or B57BL/6 mice was 209 aa or 204 aa, respectively, in length, because the latter was devoid of 5 aa in its cytoplasmic tail. We thereafter used CBA/J mouse–derived LMIR5 as mLMIR5 unless otherwise stated. Interestingly, mLMIR5 does not harbor a putative tyrosine phosphorylation site in the cytoplasmic region (Figure 1A), which is found in hLMIR5.[24]

Next, to examine the characteristics of mLMIR5 at protein levels, we generated Ba/F3 cells expressing either a Flag-tagged mLMIR5 or hLMIR5. Western blot analysis using anti-Flag mAb detected mLMIR5 as a major broad band (26-35 kDa) and a faint band (approximately 24 kDa), while hLMIR5 was detected as a broad band (27-30 kDa) and a discrete band (approximately 22 kDa) (Figure 1C). Treatment with N-glycosidase F diverted the apparent molecular mass of mLMIR5, but not hLMIR5, to several bands ranging from 22 to 26 kDa in size. This was consistent with the presence of a putative N-linked glycosylation site in the extracellular domain of mLMIR5, but not hLMIR5 (Figure 1A,C), suggesting that mLMIR5 was an N-glycoprotein.

mLMIR5 is expressed in myeloid lineage cells

To determine the tissue distribution of mLMIR5, we performed RT-PCR analysis and thereby demonstrated that mLMIR5 was

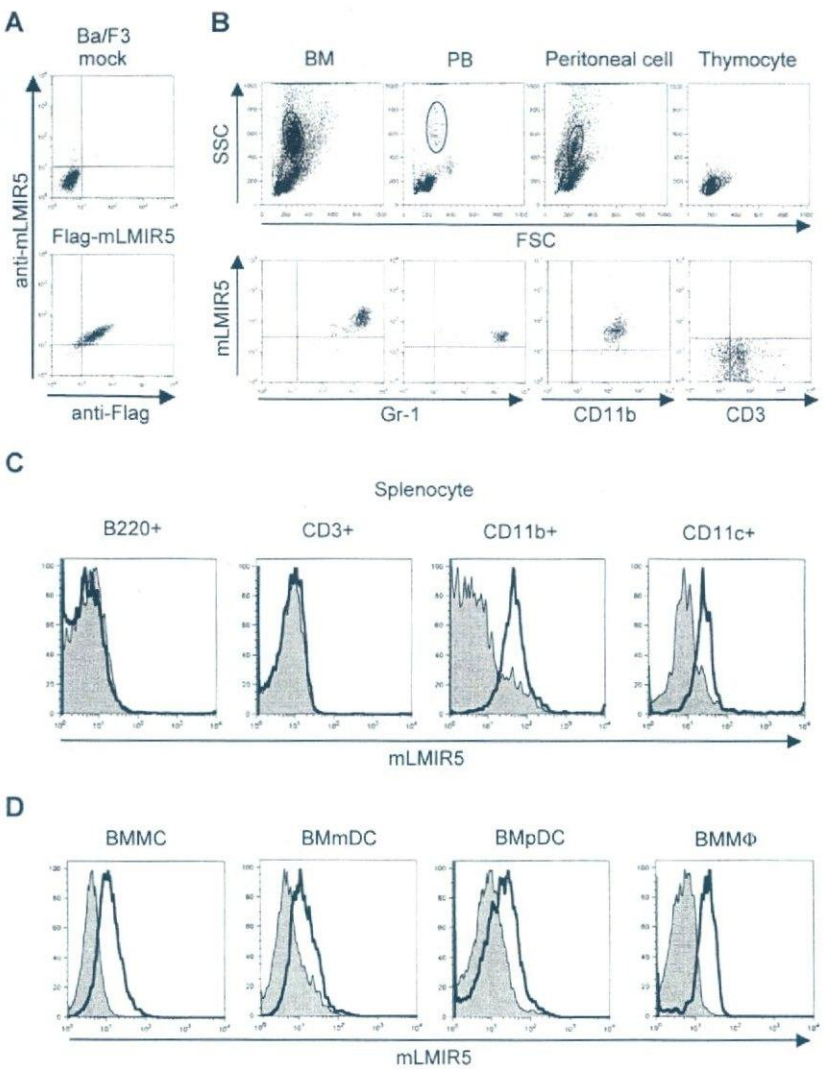

Figure 2. Cell-surface expression of mLMIR5. (A) Ba/F3 cells transduced with a Flag-tagged mLMIR5 or mock were stained with FITC-conjugated mouse IgG1 or anti-Flag Ab as well as polyclonal goat IgG or anti-mLMIR5 Ab, followed by PE-conjugated anti-goat IgG $F(ab')_2$. (B) Analysis of mLMIR5 expression on hematopoietic cells derived from C57BL/6 mice. Single-cell suspensions were prepared from BM, PB, peritoneal cavity, and thymus. Cells were stained with control IgG or anti-mLMIR5 Ab followed by PE-conjugated anti-goat IgG $F(ab')_2$ and FITC-conjugated mAbs as indicated. In BM, PB, and peritoneal cells, $FSC^{high}SSC^{high}$ populations representing myeloid lineage were gated and analyzed for mLMIR5 expression. In thymus, the $FSC^{low}SSC^{low}$ populations representing lymphoid lineage were analyzed. (C) Single-cell suspensions were prepared from spleen. After $B220^+$, $CD3^+$, $CD11b^+$, or $CD11c^+$ cells were sorted by using FITC-conjugated Abs, these cells were stained as described in panel B. (D) Analysis of mLMIR5 expression on murine BM-derived cells. BMMCs, BMmDCs, BMpDCs, and BMMΦ were stained with control IgG or anti-mLMIR5 Ab followed by PE-conjugated anti-goat IgG $F(ab')_2$. The result of control or mLMIR5 staining is shown as a filled or bold-lined histogram, respectively. All the data are representative of 3 independent experiments.

highly expressed in BM and moderately in the lung and colon (Figure 1D). Further investigation of hematopoietic cells revealed that high expression levels of mLMIR5 were observed in myeloid cell lines, including mast, macrophage, and dendritic cell lines, as well as BM-derived cells, but not in T cell lines (Figure 1E,F). Before analyzing surface expression levels of mLMIR5, we confirmed the sensitivity and specificity of polyclonal anti-mLMIR5 Ab, which recognized the extracellular domain of mLMIR5. When Ba/F3 cells were transduced with Flag-tagged mLMIR5, this Ab efficiently detected mLMIR5 on the cell surface, whose expression was confirmed by using anti-Flag mAb (Figure 2A), and anti-mLMIR5 Ab did not detect LMIR1, LMIR2, LMIR3, or LMIR4 transduced into Ba/F3 cells (Figure S1, available on the *Blood* website; see the Supplemental Materials link at the top of the online article). In addition, this polyclonal Ab and anti-Flag Ab gave a similar pattern of several bands in the Western blot of the immunoprecipitates derived from Flag-tagged mLMIR5-transduced Ba/F3 cells. Endogenous mLMIR5 in BMMCs was also detected as a similar pattern. These results confirmed the specificity of this polyclonal Ab raised against mLMIR5 (Figure S3). Surface staining of hematopoietic cell lines with anti-mLMIR5 Ab displayed the results consistent with those from RT-PCR (Figures 1E, S2); A20 cells among the B-cell lines were found to express LMIR5 in both mRNA and protein levels. We then stained a variety of hematopoietic cells using this anti-mLMIR5 Ab. When gated in the population ($FSC^{high}SSC^{high}$), immature granulocytes ($Gr\text{-}1^{high}$) in BM and macrophages ($CD11b^{high}$) in peritoneal cells displayed higher expression levels of mLMIR5, while mature granulocytes ($Gr\text{-}1^{high}$) in PB and dendritic cells ($CD11c^{high}$) in spleen showed detectable but lower expression levels as compared with immature granulocytes. However, neither B cells ($B220^{high}$) in spleen nor T cells ($CD3^{high}$) in spleen and thymus expressed mLMIR5 on their surfaces (Figure 2B,C). In addition, mLMIR5 was expressed in BM-derived cells such as BMMCs, BMmDCs, BMpDCs, and BMMΦ (Figure 2D). LMIR5 expression was also confirmed in several types of mast cells, including peritoneal mast cells and FLMCs (Figure 2D; data not shown). Collectively, mLMIR5 was mainly expressed in myeloid cells.

mLMIR5 associates strongly with DAP12 and to a lesser extent with DAP10 in mLMIR5-transduced cells

The presence of a positively charged residue (lysine) in the transmembrane suggested that LMIR5 associated with adaptor

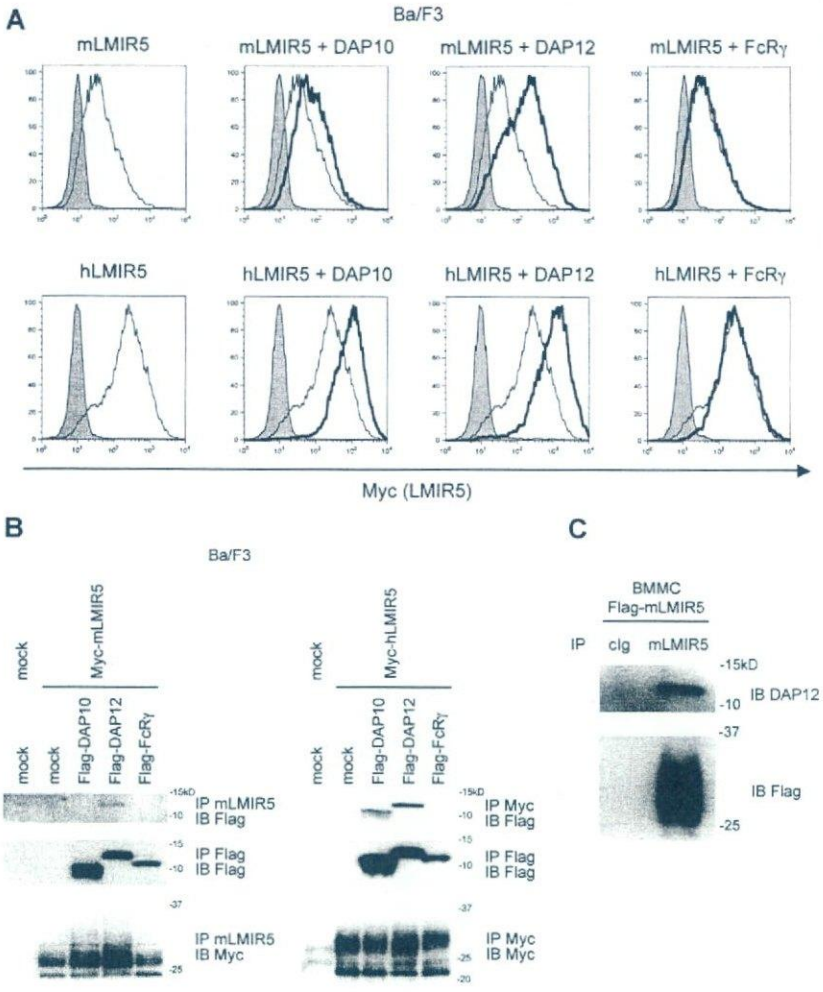

Figure 3. Association of LMIR5 with adaptor molecules such as DAP10, DAP12, and FcRγ. (A,B) Ba/F3 cells were cotransduced with a Myc-tagged mLMIR5 or hLMIR5 and either a Flag-tagged DAP10, DAP12, FcRγ, or mock. (A) Cell-surface expression levels of mLMIR5 (top row) or hLMIR5 (bottom row) were analyzed by flow cytometry by staining cells with control mouse IgG1 or anti-Myc mAb, followed by FITC-conjugated anti-mouse Ig polyclonal Ab. The result of LMIR5 staining in the presence or absence of indicated adaptor molecule was represented by bold- or thin-lined histograms, respectively, while that of control staining was represented by a filled histogram. (B) Lysates of trasduced-Ba/F3 cells were immunoprecipitated with anti-mLMIR5 Ab, anti-Myc Ab, or anti-Flag mAb, and then immunoblotted with anti-Flag mAb or anti-Myc mAb. (C) Lysates of mLMIR5-transduced BMMCs were immnoprecipitated with control IgG or anti-mLMIR5 Ab, and then immunoblotted with anti-DAP12 Ab or anti-Flag mAb.

molecules—such as DAP10, DAP12, and FcRγ—containing a negatively charged residue within the transmembrane domain. To test this, we generated Ba/F3 cells cotransfected with retroviruses expressing a Myc-tagged mLMIR5 or hLMIR5 together with either a Flag-tagged DAP10, DAP12, FcRγ, or mock. Transduction of either mLMIR5 or hLMIR5 did not alter the expression levels of DAP10 and DAP12 mRNA when tested by real-time PCR (data not shown). Staining of these transfectants with anti-Myc mAb revealed that surface expression levels of mLMIR5 were significantly lower than those of hLMIR5 when LMIR5 was expressed alone. Surface expression levels of mLMIR5 were weakly or strongly elevated by DAP10 transduction or DAP12 transduction, respectively, while those of hLMIR5 were elevated by DAP10 as efficiently as by DAP12 (Figure 3A). The transduction of FcRγ did not influence the surface expression levels of mLMIR5 and hLMIR5 (Figure 3A). To confirm the physical association of mLMIR5 with either DAP10 or DAP12, we performed coimmunoprecipitation experiments; DAP12, but not DAP10, was coimmunoprecipitated with mLMIR5 probably because mLMIR5 more strongly associated with DAP12 compared with DAP10. On the other hand, total expression levels of mLMIR5 were elevated by the transduction of either DAP10 or DAP12, suggesting that these adaptors stabilized mLMIR5. When similar experiments were conducted on hLMIR5, both DAP10 and DAP12 were coimmunoprecipitated with hLMIR5 (Figure 3B). Furthermore, coimmunoprecipitation of endogenous DAP12 with transduced mLMIR5 was observed in BMMCs (Figure 3C). In conclusion, mLMIR5 was capable of associating strongly with DAP12 and to a lesser extent with DAP10, at least in mLMIR5-transduced cells.

Cross-linking of mLMIR5 induces the activation of mast cells

Since mLMIR5 was highly expressed in mast cells, we analyzed the activating functions of mLMIR5 in BMMCs. To obtain strong activation, mLMIR was transduced into BMMCs. When mLMIR5 was engaged by anti-mLMIR5 Ab, but not control Ab, in mLMIR5-transduced BMMCs, strong activation of ERK, p38, and Akt was recognized by using phospho-specific Abs, indicating a cellular activation in mast cells stimulated by LMIR5 cross-linking (Figure 4A). Mast cells, when activated by FcεRI aggregation, cause a variety of activation events such as cytokine/chemokine production and degranulation characterized by histamine release.[1,3,25,36-38] Therefore, we performed experiments to examine whether similar activation events were induced by mLMIR5 engagement. In line with cellular activation, mLMIR5-transduced BMMCs stimulated by anti-mLMIR5 Ab, but not control Ab, produced IL-6, TNF-α, and MCP-1 (Figure 4B), and adhered efficiently to fibronectin or fibrinogen (Figure 4C). On the other hand, degranulation or cell

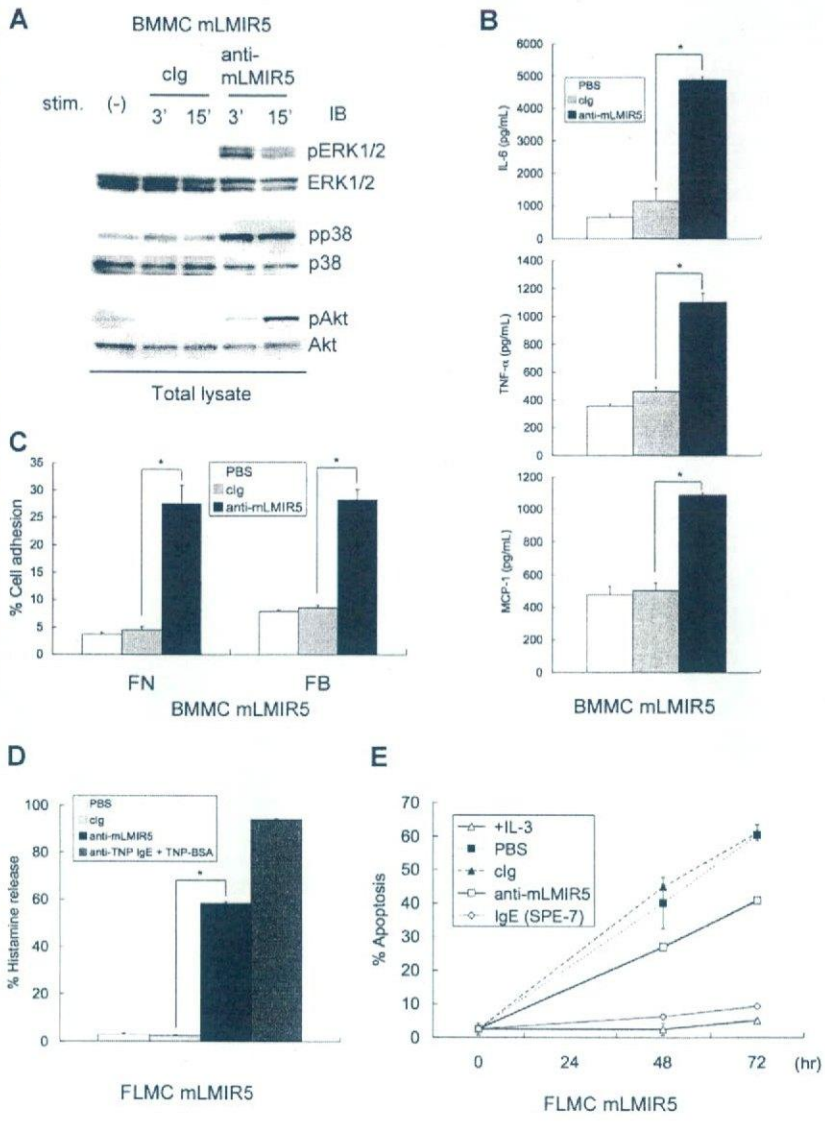

Figure 4. Cross-linking of mLMIR5 induced the phosphorylation of several signaling molecules in mLMIR5-transduced mast cells, resulting in cytokine/chemokine production, cell adhesion, histamine release, and cell survival. (A) BMMCs transduced with mLMIR5 were stimulated with either control IgG or anti-mLMIR5 Ab for 3 or 15 minutes. Cell lysates were subjected to immunoblotting with either anti–phospho-p44/42 MAPK (pERK1/2), anti–phospho-p38 MAPK (pp38), or anti–phospho-Akt (pAkt) Ab. Equal loading was evaluated with by reprobing the immunoblots with Abs specific for ERK1/2, p38, or Akt. (B) BMMCs transduced with mLMIR5 were incubated with PBS, control IgG, or anti-mLMIR5 Ab for 12 hours. IL-6, TNF-α, and MCP-1 released into the culture supernatants were measured by ELISA. (C) BMMCs transduced with mLMIR5 in FN- or FB-coated plates were stimulated with PBS, control IgG, or anti-mLMIR5 Ab for 60 minutes. Adherent cells were measured as described in "Measurement of cytokines and histamines and adhesion assay." (D) FLMCs transduced with mLMIR5 were incubated with PBS, control IgG, or anti-mLMIR5 Ab for 50 minutes. Alternatively, anti-TNP IgE-sensitized cells were incubated with TNP-BSA for 50 minutes. Histamine released in the culture supernatants was measured. (E) FLMCs transduced with mLMIR5 were incubated with either PBS, control IgG, anti-mLMIR5 Ab, or IgE (SPE-7) in the absence of IL-3. At indicated time points, cells were stained with PE-labeled annexin V to monitor apoptosis. Cells incubated in the presence of IL-3 were also analyzed. All data points correspond to the mean and the standard deviation (SD) of 4 independent experiments. Statistically significant differences are shown. $^*P < .05$.

survival effect was significant but weak in mLMIR5-transduced BMMCs stimulated by anti-mLMIR5 Ab (data not shown). Importantly, mLMIR5-transduced FLMCs in response to anti-mLMIR5 Ab stimulation efficiently released histamine and showed an antiapoptotic effect under IL-3–depleted conditions, thus demonstrating that engagement of endogenous mLMIR5 could also activate the cellular responses (Figure 4D,E).[25,39,40] Taken together, mLMIR5 functioned as an activating receptor in mast cells.

DAP12 is required for the activation induced by mLMIR5 engagement as well as the sufficient surface expression of mLMIR5 under physiologic conditions

To determine which adaptor protein was a physiologic partner of mLMIR5, we analyzed surface expression levels of mLMIR5 in BM cells or BMMCs derived from wild-type (WT), *DAP10*$^{-/-}$, *DAP12*$^{-/-}$, or *FcRγ*$^{-/-}$ mice.[20,22,23,28,29,41] As depicted in Figure 5A, surface expression levels of mLMIR5 in BM granulocytes derived only from DAP12-deficient mice were reduced when compared with those from other mice. On the other hand, surface expression levels of mLMIR5 in BMMCs were strongly or moderately reduced by DAP12 or DAP10 deficiency, respectively (Figure 5B). To further address the dependency of activating events caused by mLMIR5 aggregation on each adaptor protein, mLMIR5 was transduced into these BMMCs. The transduced cells exhibited comparable expression levels of FcεRI and c-kit in addition to transduced mLMIR5, irrespective of the deficiency of respective adaptor molecule (Figure 5C bottom row). FcεRI expression was not detectable in FcRγ-deficient BMMCs as reported (Figure 5C top row).[29,41] Importantly, DAP12- or DAP10-deficient BMMCs in response to mLMIR5 engagement exhibited negligible or weak, respectively, activation of ERK as compared with WT BMMCs (Figure 5D), in proportion to the decreased capacities of DAP12- or DAP10-deficient BMMCs to adhere to fibronectin (Figure 5E). Concurrently, we confirmed that adhesion levels caused by PMA stimulation were comparable among these transfectants, and that FcRγ-deficient BMMCs did not adhere in response to IgE because of the lack of FcεRI on the cell surface, as expected (Figure 5E). Although the deficiency of adaptor molecules did not show any morphologic difference in mast cells (data not shown), real-time PCR analysis demonstrated significantly low expression levels

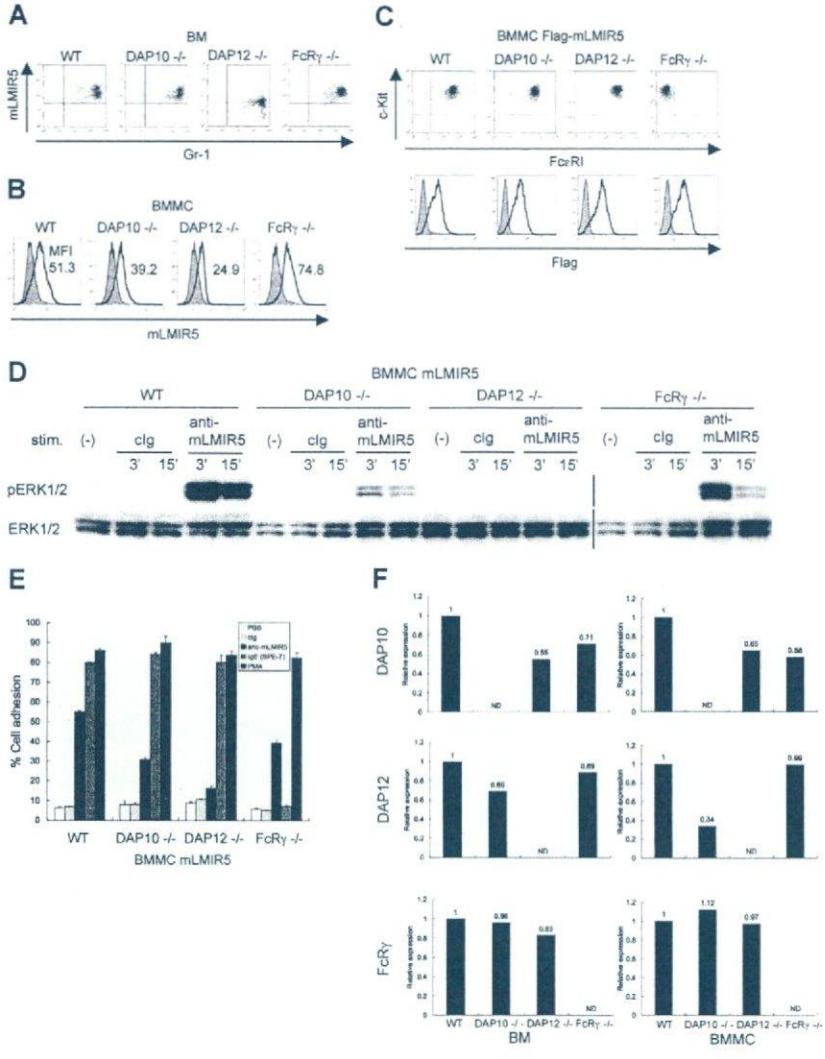

Figure 5. Analysis of BM cells and BMMCs derived from *DAP10*$^{-/-}$, *DAP12*$^{-/-}$, and *FcRγ*$^{-/-}$ mice. (A,B) Surface expression levels of endogenous mLMIR5 on BM cells and BMMCs derived from WT, *DAP10*$^{-/-}$, DAP12$^{-/-}$, or FcRγ$^{-/-}$ mice were analyzed as described in Figure 2. The mean fluorescent intensity (MFI) of mLMIR5 expression was indicated in BMMCs. (C) WT, *DAP10*$^{-/-}$, DAP12$^{-/-}$, or *FcRγ*$^{-/-}$ BMMCs transduced with Flag-tagged mLMIR5 were stained with control IgG or anti-Flag mAb followed by FITC-conjugated anti-mouse Ig Ab to confirm transduced-mLMIR5 expression levels (bottom row). Phenotypical analysis of BMMCs was performed as described in materials and methods (top row). (D) Either WT, *DAP10*$^{-/-}$, DAP12$^{-/-}$, or *FcRγ*$^{-/-}$ BMMCs transduced with mLMIR5 were stimulated with control IgG or anti-mLMIR5 Ab. The amount of phosphorylated ERK1/2 was analyzed as described in Figure 4A. Vertical lines have been inserted to indicate a repositioned gel lane. (E) Either WT, *DAP10*$^{-/-}$, DAP12$^{-/-}$, or *FcRγ*$^{-/-}$ BMMCs transduced with mLMIR5 were stimulated on FN-coated plates. Percentages of adherent cells were estimated. All data points correspond to the mean and the SD of 3 independent experiments as indicated. (F) Relative expression levels of DAP10, DAP12, and FcRγ among WT, *DAP10*$^{-/-}$, DAP12$^{-/-}$, and *FcRγ*$^{-/-}$ BM or BMMCs were estimated by using real-time PCR as described in "Gene expression analysis." The amount of expression was indicated relative to that in wild-type BM or BMMCs. Data are representative of 3 independent experiments.

(approximately 30%) of DAP12 in DAP10-deficient BMMCs and decreased expression levels of DAP10 (approximately 60%) in DAP12- or FcRγ-deficient BMMCs, when compared with those in WT BMMCs (Figure 5F right panel). On the other hand, expression levels of DAP12 in DAP10-deficient BM were approximately 70% of those in WT BM (Figure 5F left panel). Considering the recent report that DAP12 transcript levels were not altered by DAP10 deficiency,[20,22] expression levels of DAP12 might have been decreased during the course of differentiation of DAP10-deficient BMMCs in culture. Thus, attenuated activation induced by mLMIR5 cross-linking as well as reduced surface expression levels of mLMIR5 in DAP10-deficient BMMCs can be explained by the decreased expression levels of DAP12 rather than by the deficiency of DAP10. In summary, DAP12 plays a major role in maintaining surface expression levels of mLMIR5 under physiologic conditions and in transmitting activating signals induced by mLMIR5 aggregation.

Different signaling pathways between mLMIR5 and hLMIR5

To explore whether the activating functions of hLMIR5 are also regulated by DAP12, Flag-tagged hLMIR5 was transduced into WT or DAP12-deficient BMMCs. Surprisingly, DAP12 deficiency did not inhibit but rather enhanced IL-6 production caused by hLMIR5 cross-linking (Figure 6A bottom row), while it completely abrogated that by mLMIR5 cross-linking (Figure 6A top row), notwithstanding equivalent amounts of cytokine production of WT and DAP12-deficient transfectants stimulated by PMA (Figure 6A). This was consistent with the finding that LMIR5 cross-linking induced strong activation of ERK in DAP12-deficient BMMCs transduced only with hLMIR5, but not mLMIR5 (Figure 6B), and that ERK activation induced by cross-linking of transduced hLMIR5 was rather enhanced in DAP12-deficient BMMCs in comparison with that of WT BMMC (Figure 6C). Since hLMIR5, but not mLMIR5, contained the putative phosphorylation site (Y188) in the cytoplasmic tail, we asked if this is related to DAP12-independent activation of mast cells stimulated by hLMIR5 cross-linking. Intriguingly, the phosphorylation of hLMIR5 was observed only in DAP12-deficient, but not WT, mast cells in response to hLMIR5 aggregation (Figure 6C). To further confirm that Y188 of hLMIR5 was indeed phosphorylated, we transduced either mock, Flag-tagged hLMIR5, or Flag-tagged hLMIR5 (Y188F) into WT BMMCs. As demonstrated in Figure 6D, stimulation of BMMCs with pervanadate induced tyrosine phosphorylation of hLMIR5, but not hLMIR5 (Y188F), suggesting that Y188 was a

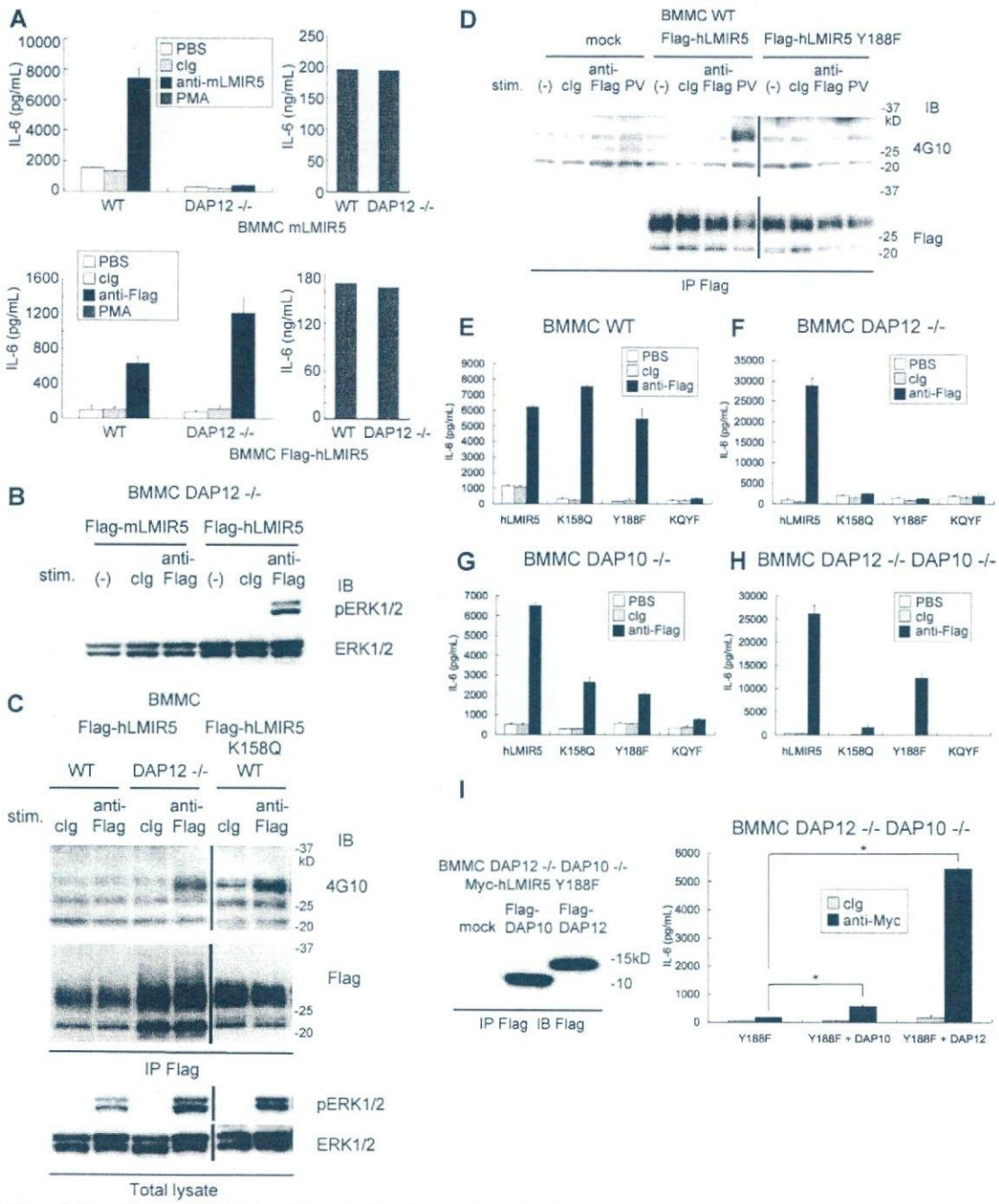

Figure 6. Cross-linking of human LMIR5 induced the activation via phosphorylation of Y188 in its cytoplasmic region in DAP12-deficient BMMCs. (A) WT or *DAP12*$^{-/-}$ BMMCs transduced with a Flag-tagged mLMIR5 were stimulated with control IgG, anti-mLMIR5 Ab, or PMA (top panels), while WT or *DAP12*$^{-/-}$ BMMCs transduced with Flag-tagged hLMIR5 were stimulated with control IgG, anti-Flag mAb, or PMA (bottom panels). IL-6 released into the culture supernatants was measured by ELISA. All data points correspond to the mean and the SD of 4 independent experiments. (B) *DAP12*$^{-/-}$ BMMCs transduced with either a Flag-tagged mLMIR5 or hLMIR5 were stimulated with the indicated Abs for 3 minutes. The amount of phosphorylated ERK1/2 was analyzed as described. (C) WT or *DAP12*$^{-/-}$ BMMCs transduced with Flag-tagged hLMIR5 or WT BMMCs transduced with Flag-tagged hLMIR5 (K158Q) were incubated with the indicated Abs. Immunoprecipitates of cell lysates with anti-Flag mAb were immunoblotted with anti-phosphotyrosine mAb (4G10) or anti-Flag mAb. Total cell lysates were also analyzed to detect the amount of phosphorylated ERK1/2. Vertical lines have been inserted to indicate a repositioned gel lane. (D) BMMCs transduced with Flag-tagged hLMIR5, hLMIR5 (Y188F), or mock were stimulated with the indicated Ab for 3 minutes or with 100 μm pervanadate (PV) for 10 minutes. Immunoprecipitates of cell lysates with anti-Flag mAb were blotted with antiphosphotyrosine mAb (4G10) or anti-Flag mAb. Vertical lines have been inserted to indicate a repositioned gel lane. (E-H) WT (E) or *DAP12*$^{-/-}$ (F) *DAP10*$^{-/-}$ (G), or *DAP12*$^{-/-}$*DAP10*$^{-/-}$ (H) BMMCs transduced with Flag-tagged hLMIR5, hLMIR5 (K158Q), hLMIR5 (Y188F), or hLMIR5 (K158Q) (Y188F) were stimulated with control IgG or anti-Flag mAb. IL-6 released into the culture supernatants was measured by ELISA. All data points correspond to the mean and the SD of 3 independent experiments. K158Q, Y188F, or KQYF indicate hLMIR5 (K158Q), hLMIR5 (Y188F), or hLMIR5 (K158Q) (Y188F), respectively. (I) *DAP12*$^{-/-}$*DAP10*$^{-/-}$ BMMCs transduced with Myc-tagged hLMIR5 (Y188F) were transfected with Flag-tagged DAP10, DAP12, or mock. Immunoprecipitates of cell lysates were immunoblotted with anti-Flag mAb (left panel). These cells were stimulated with control IgG or anti-Myc mAb. IL-6 released into the culture supernatants was measured by ELISA. All data points correspond to the mean and the SD of 3 independent experiments. Statistically significant differences are shown. *$P < .05$.